Micropetrology: are inclusions grains of truth?

Silvio Ferrero[1,2*] & Ross Angel[3]

[1] Institut für Erd- und Umweltwissenschaften, Universität Potsdam, 14476 Potsdam, Deutschland.

[2] Museum für Naturkunde (MfN), Leibniz-Institut für Evolutions- und Biodiversitätsforschung, 10115 Berlin, Deutschland

[3]Department of Earth and Environmental Sciences, University of Pavia, Via Ferrata 1, 27100, Pavia, Italy. rossjohnangel@gmail.com

*Corresponding Author: E-mail sferrero@geo.uni-potsdam.de

ABSTRACT

Inclusions in minerals, whether fluids, melts or crystalline phases, are small pieces of the large-scale puzzle of Nature, time-consuming to investigate and often of difficult interpretation. Yet they are windows into the past of their host mineral. Mineral inclusions provide the opportunity to unravel the genesis of their host, whilst the increasingly refined understanding of their elastic behaviour provides the basis for alternative, equilibrium-independent geobarometry. Fluid and melt inclusions reveal information about material transfer in the Earth system, from shallow mineralization to mantle re-fertilization via subduction. The study of inclusions is thus one of the most intriguing and fertile branches of

micropetrology. In this contribution, we focus on two recent developments: the use of elasticity models to extract the formation conditions of the host crystal, and the discovery and investigation of melt inclusions in metamorphic rocks. We also discuss how to evaluate the information provided by inclusions, given that they are no longer at the pressure and temperature conditions of entrapment. We discuss how to understand and quantify the changes undergone during cooling and depressurisation, and how metastability-related phenomena in inclusions, such as crystallization of rare polymorphs, and preservation of the original content of volatiles in fluid and melt inclusions, provide direct evidence that inclusions represent closed systems. The field of study of inclusions in minerals still has a largely-untapped potential. The most fruitful avenues for future research will emerge from continuous technological innovation in analytical and imaging techniques, the application of experimental petrology, and the development and application of new theoretical models for coupled mineral behaviour under changing *P-T* conditions.

KEYWORDS: inclusions, nanogranitoids, polymorphs, elastic geobarometry

INTRODUCTION

"*There is no necessary connexion between the size of an object and the value of a fact, and … though the objects I have described are minute, the conclusions to be derived from the facts are great.*"

H.C. Sorby (1858)

Inclusions are portions of material – minerals, fluids and melts - trapped in larger crystals during either their formation or recrystallization. Inclusions represent a very limited portion of any volume of rock and, as a result, they are often disregarded as minor, even negligible,

sources of information when compared to the much larger-scale puzzle of Nature. As H.C. Sorby pointed out 150 years ago, this is a mistaken perception. The micro-universe and processes at the macro-scale all belong to the same continuum, and the comprehension of their mutual relationships holds the key to fully understanding the whole Earth system.

From the moment of their entrapment, inclusions live in a different world with respect to their surrounding environment. Sheltered in the host crystal, they are generally isolated from most of the physico-chemical changes affecting rocks at depth. Hence, inclusions in minerals are likely to preserve information about the formation of the host crystal. They may provide completely independent, often unique, insights into the protoliths and *P-T* paths of metamorphic rocks. Inclusions of diamonds (first discovered by Sobolev & Shatsky, 1990) and coesite (first reported by Chopin, 1984) enclosed in metamorphic garnet are often the only direct mineralogical evidence of an ultra-deep metamorphic history (e.g. Majka *et al*., 2014; Klonowska *et al*., 2017). The discovery of these UHP phases in crustal rocks provides an excellent example of how the study of mineral inclusions may cause paradigm shifts, e.g., leading to the theory that continental crust can be subducted to depths of more than 100 km in collisional orogens (Spear *et al.* 2016). However, as our understanding of Nature continuously evolves, the equation diamond/coesite = deep crustal subduction is already under fire, with the advent of new theories to explain the presence of UHP phases in crustal rocks. Tectonic overpressure (e.g. Schmalholz & Podladchikov, 2013, 2014), confined melting (e.g Vrijmoed *et al.* 2009), and local over-pressurization at the grain scale (e.g. Tajčmanová *et al.* 2014, 2015) have all been invoked as alternative genetic processes.

Any mineral can trap and preserve any of the phases present in its surroundings during its (re)crystallization, whether melt, fluid or other minerals. Thus, inclusions are a ubiquitous feature of natural rocks Inclusions of fluids and melts provide possibly the most obvious example of how fundamental inclusions are for unravelling rock histories. Fluids involved in geological processes are highly mobile and easily modified (e.g. Yardley, 2009; Jamtveit &

Austrheim, 2010; Connolly, 2010), often completely lost during cooling, crystallization and, or, deformation; only when preserved as inclusions can they be directly investigated. Fluid inclusions (FI) have shaped our knowledge of natural processes since the end of the 17th century, when Robert Boyle observed a large moving bubble in quartz (Boyle (1672), as reported by Roedder, 1984), and the presence of fluid inclusions in quartz was used to support the Neptunist theory that proposed that crystals and rocks directly precipitate from water (Newcomb, 2009; see also Roedder *et al*., 1984).

The investigation of inclusions of melt (MI) dates from Sorby's work (Sorby, 1858). In the last decade, MI have also been recognized in partially-melted crustal rocks (Cesare *et al*. (2015) provide a comprehensive review), providing a powerful way of circumventing the problems of preservation of buoyant anatectic melts that are commonly mostly removed from their source (Sawyer *et al*. 2011; Yakymchuk & Brown, 2014), particularly during syn-melting deformation (Brown, 2007). In igneous environments, magma de-gassing leads to the loss of most volatiles during eruption or crystallisation at shallow crustal levels. Only when fluids and melts are trapped to form inclusions within (re)crystallizing phases can we directly characterize them.

In summary, inclusions can tell us a lot of stories about the Earth's evolution, although their full potential is still only partially tapped. Are we able to read these stories and understand them correctly? How much of what inclusions tell us should we believe? In a nutshell, to what extent are inclusions really "grains of truth"? In this contribution, we address these questions in the light of recent developments and results. We first review the thermodynamics of inclusion systems to emphasise the common principles of behaviour of MI, FI and solid inclusions, and show where they differ fundamentally from the thermodynamics of an open system. Then we show how these concepts can be applied to the understanding of single-phase mineral inclusions as a basis for interpreting the more complex

situations found in melt inclusions, to provide insights into the geological history of the rocks in which they are found.

Recent reviews have summarized and discussed the information provided by different types of inclusion (see, for example, Audetat & Lowenstern (2014) on igneous melt inclusions; Frezzotti & Ferrando (2015) on deep fluids; Cesare *et al*. (2015) on anatectic MI; and Gao *et al*. (2017) on deep melts), whereas the current state of inclusions in metamorphic petrology has recently been discussed by Spear *et al*. (2016). Therefore, here we will focus on two of the most recent developments in the field of inclusion studies: (1) the development of elasticity models to extract the formation conditions of the host crystal; (2) the discovery and petrological-experimental investigation of MI in metamorphic rocks.

THERMODYNAMICS OF INCLUSIONS

The fundamental differences in the behaviour of all inclusions compared to the same material in the matrix of the rock arise from the fact that the inclusion is protected *and* constrained by the host mineral. We first show the consequences for the pressure of a single phase inclusion, and then we discuss the implications for phase equilibria, reactions and transitions within the inclusion. In all of this we assume that the thermal conductivity of the host mineral is sufficiently large that the host and inclusion are always at the same temperature. This is valid for most geological processes except those involving shock heating, for example due to faulting or meteorite impacts (e.g. Papa *et al*., 2018; French & Koeberl, 2010).

Inclusion pressures

Remanent stresses in an inclusion are developed because the inclusion and the host have different thermal expansions and compressibilities, and the inclusion cannot expand in response to P and T as would a free crystal. Instead, it is restricted to expand only as much as

the host mineral allows, and this constriction in volume can result in inclusions exhibiting over- or under-pressures when the host is studied at room conditions (Rosenfeld & Chase 1961). Remnant stresses in inclusions therefore derive from an elastic effect. The inclusion stress state may also be modified by other processes such as plastic flow or brittle failure (discussed below), but they are driven by the elastic stresses.

Elastic processes are, by definition, reversible, and calculations of elastic stresses can be made over any convenient path in *P-T* space, between entrapment conditions and any subsequent condition of interest. Therefore, the thermodynamic concept of an *isomeke* (Rosenfeld & Chase 1961; Adams *et al.* 1975) can provide a useful basis for understanding the thermodynamics of inclusions. The use of the isomeke in calculations is only a convenience; it does not imply that the host-inclusion system in a rock actually followed the isomeke on exhumation.

Garnet-diamond host-inclusion systems can serve to illustrate the thermodynamic principles. From the volume equations of state of the two minerals one can calculate isomekes in *P-T* space, along which the fractional volume change of the host and inclusion remain the same (Fig. 1a). The slope of an isomeke is $\left(\frac{\partial P}{\partial T}\right)_{isomeke} = \frac{\alpha_{\mathrm{I}} - \alpha_{\mathrm{H}}}{\beta_{\mathrm{I}} - \beta_{\mathrm{H}}}$, and depends on the contrast between the thermal expansion coefficients of the inclusion and host, $(\alpha_{\mathrm{I}} - \alpha_{\mathrm{H}})$, and the contrast in volume compressibilities $(\beta_{\mathrm{I}} - \beta_{\mathrm{H}})$. This relationship applies equally to FI and MI, and to inclusions of more than one phase. Note that the isomeke is *not* an isochor of either phase, but it reduces to the isochor for the inclusion if the host is completely rigid with $\alpha_{\mathrm{H}} = \beta_{\mathrm{H}} = 0$. The successful approximation of isochoric behaviour for fluid inclusions arises from $\alpha_{\mathrm{I}} >> \alpha_{\mathrm{H}}$ and $\beta_{\mathrm{I}} >> \beta_{\mathrm{H}}$.

If a garnet is trapped inside a diamond during diamond growth, and the garnet completely fills the space inside the diamond, then the isomeke line through the *P-T* conditions of entrapment also defines the set of *P* and *T* at which the inclusion remains at the

same pressure as the external pressure (Fig. 1a). This entrapment isomeke thus divides *P-T* space into two regions. On one side the inclusion will exhibit higher pressures than the external pressure on the host mineral. On the other side of the entrapment isomeke the pressure in the inclusion will be less than the external pressure. Whether the inclusion is over- or under-pressured, with respect to the external pressure on the host, is determined by the contrast in the bulk moduli, $K = -V\frac{\partial P}{\partial V} = \frac{1}{\beta}$, of the host and inclusion. The pressure change in the inclusion, dP_{inc}, due to the host moving off the entrapment isomeke by an isothermal pressure change of dP_{ext}, is given in the linear infinitesimal limit as $dP_{inc} = \frac{K_{inc}}{K_{host}} dP_{ext}$. The consequence is that for a relatively soft inclusion, such as a garnet in a stiff diamond (i.e. $\frac{K_{inc}}{K_{host}} < 1$), the pressure of the inclusion always remains between the external pressure and the pressure of the entrapment isomeke. For a garnet trapped in a diamond that grew within the thermodynamic stability field of diamond, the entrapment isomeke is always at P > 0 at room temperature (Fig. 1a) for entrapment in the crust or upper mantle. Because room pressure lies below the isomeke, when the host diamond is at room pressure and temperature, the garnet inclusion must exhibit an over-pressure ($P_{inc} > P_{ext} \sim 0$), as observed in un-cracked garnet inclusions (e.g. Howell *et al.* 2010; Milani *et al.* 2015; Kueter *et al.* 2016).

For the opposite case of diamond inclusions inside garnets trapped at *P* and *T* within the stability field of diamond, $K_{inc} > K_{host}$, and therefore the sense of the pressure difference between the inclusion and the external pressure is reversed (Fig 1b). Decompression from the same entrapment isomeke at room temperature then leads to $dP_{inc} > dP_{ext}$. Therefore, when the garnet host is at room conditions ($P_{ext} \sim 0$) thermodynamics predicts that the diamond inclusion should be under negative pressure (Fig. 1b). In the absence of bonding between the garnet and diamond surfaces, this means that void space would be developed at the diamond-

garnet interface, the diamond would "rattle" in the hole of the garnet, and it would thus be at room pressure.

Elastic Relaxation

If the constriction of the inclusion to follow the volume changes of the host were the only contribution to the inclusion P, then the latter could be simply calculated from the equation of state (EoS) of the two minerals; a simple thermodynamic problem that leads to the calculation of a 'thermodynamic pressure' for the inclusion that we call P_{thermo}. However, as we have seen above, this P_{thermo} is always different from the external pressure as soon as the host-inclusion system leaves the isomeke of entrapment. The difference between P_{thermo} and P_{ext} drives an additional immediate elastic relaxation of the host-inclusion boundary that *always* reduces the pressure difference between the inclusion and the external pressure. The change in inclusion P from P_{thermo} is called ΔP_{relax}. As an elastic process it is instantaneous, and therefore no inclusion ever exhibits a pressure of P_{thermo}, except in the trivial situation when the host is on the entrapment isomeke when $P_{thermo} = P_{ext}$ and $\Delta P_{relax} = 0$.

The isomeke is also then the key concept for the quantitative calculation of inclusion P_{inc} because it provides, for cubic hosts and inclusions, a state of uniform stress at the final T and thus a basis for the exact calculation of ΔP_{relax} (Angel *et al*. 2014b; Angel *et al*. 2017a). The theory is physically complete and correct, but exact calculations can only be performed for isolated spherical inclusions of an elastically isotropic material within a much larger elastically isotropic host (Rosenfeld & Chase 1961). The magnitude of ΔP_{relax} depends on the contrast in the elastic properties of the host and the inclusion, the shear modulus of the host and the difference between the final external pressure on the host and the pressure on the entrapment isomeke at the final temperature (Angel *et al*., 2017). Figure 2a shows the evolution of P_{thermo} inside a coesite inclusion trapped in a garnet, and the inclusion pressure if

the coesite inclusion were isotropic (which it is not) and spherical. Because the late-stages of exhumation follow a *P-T* path that is almost perpendicular to the entrapment isomeke, quite large inclusion over-pressures are developed (Fig. 2a).

Phase Equilibria in Inclusions

Equilibrium thermodynamics as used in petrology assumes free boundary conditions, with the rock volume free to expand at constant *P* and *T*. Even if it is not clear that this is generally a valid boundary condition for rocks (e.g. Mancktelow, 1995; Vrijmoed *et al.* 2009; Hacker & Gerya, 2013 Moulas *et al.* 2013, Tajčmanová *et al.* 2014, 2015), it is certainly not valid for an inclusion because it is enclosed by the host mineral and is therefore not free to expand. As a consequence of thermal equilibration on the crystal length-scale being fast compared to most geological timescales, the thermodynamic equilibrium behaviour of the inclusion is governed by the external *T* and the volume imposed by the host crystal, together with the mutual elastic relaxation. Thus, P_{inc} becomes a dependent variable for the thermodynamics of an inclusion.

A simple example is provided by melting. Melting in a rock matrix as a result of an increase in *T* leads to an increase in volume and a decrease in density at constant *P*. In contrast, melting of a constrained system such as that of a crystallized melt inclusion does not change the density of the inclusion itself. Its chemistry and its volume are kept approximately constant by encapsulation, with small changes arising only from thermal expansion of the host and changes in the relaxation. Therefore melting of an inclusion leads to a pressure increase in the inclusion (see also Vrijmoed *et al.* 2009). This is clearly visible when crystallised former melt inclusions are experimentally heated to melting *T* without applying any confining pressure, for example in a classic heating stage used for magmatic MI studies (Audetát & Lowenstern, 2014). As the crystalline phases in the inclusion start to melt, the internal *P* of the inclusion rises until it very often overcomes the strength of the host mineral: the result is the failure of the host mineral, with more or less extensive decrepitation and material loss

(Bartoli *et al.*, 2013a; Ferrero *et al.* 2012; Cesare *et al.* 2015). Therefore, in order to obtain bulk chemical analyses of partially crystallised MI, they must be re-melted under a confining pressure to prevent decrepitation. The pressure required to obtain re-homogenisation of a MI without decrepitation places a lower bound on the original entrapment pressure (Ferrero *et al*. 2018b).

If there were no elastic relaxation, the stable phase assemblage in an inclusion would be the one with the lowest Helmholtz free energy, in contrast to the assemblage with the lowest Gibbs free energy in the rock matrix. With relaxation, neither free energy is an appropriate predictor of the equilibrium phase assemblage in an inclusion. The equilibrium thermodynamic consequences of inclusion entrapment therefore often appear to represent metastable equilibrium when viewed from the perspective of the rock as a whole. The simplest example is provided by polymorphic transitions in silica. Mineral inclusions such as quartz have thermal expansion coefficients that are similar to the host garnets, so the isomeke slopes tend to be shallow in *P*-*T* space. Consequently, the pressures in quartz inclusions originally entrapped in garnet cores during the early stages of subduction lag so far behind the external *P* that they often do not pass into the stability field of coesite, even when the garnet is at peak *P* (for details of the calculation see Angel *et al.* 2015b). The apparent metastability of quartz in garnet at pressures in the coesite field is thus just a consequence of the contrast of elastic properties of the host and inclusion and the constrained state of the inclusion, and it actually represents equilibrium thermodynamics.

The same elastic effects are also responsible for the apparent metastable preservation of high-pressure phases as inclusions. For example, after entrapment of a coesite grain at 3.7 GPa and 800 °C, a host pyrope garnet will expand by just 0.15% in volume on recovery to room conditions. Constraining the coesite, which has a much lower bulk modulus, to only expand by this amount would mean that its pressure (P_{thermo}) would be ~2.8 GPa at room temperature, leaving it in the coesite stability field (Fig. 2a). Thus, we would not expect any

transformation of trapped coesite to quartz in a pristine inclusion in garnet. (Note that the exact pressures and volume changes quoted here depend on the exact P and T of entrapment, but the conclusions are general). However, this example also illustrates the importance of calculating the correct pressure relaxation, ΔP_{relax}, driven by large pressure contrast between the P_{thermo} (2.8 GPa) and the ambient P on the garnet when examined in the laboratory (Angel *et al.* 2014a, 2017a). This relaxation is ~1.2 GPa, which drops the final inclusion P to ~1.6 GPa within the stability field of quartz, well below the quartz-coesite phase boundary (Fig. 2a). The inclusion over-pressures and associated deviatoric stresses in the garnet that build up during exhumation often crack the host garnet. Infiltration of fluids, generally present in rocks during retrogression, can catalyse the inversion to quartz, and the coesite to quartz reaction then proceeds within the controlled volume of the inclusion. Whereas in single-phase inclusions the expansion of the host during decompression is accommodated by a change in the inclusion P, the reaction of more coesite to quartz provides the volume expansion and the inclusion P remains buffered to that of the transition boundary (Fig. 2b). The same phenomenon of pressure buffering is observed in experimental apparatus where the sample volume is externally constrained (e.g. Arlt & Angel, 2000). Because the volume change of the garnet to room P is not sufficient to allow all the coesite to invert to quartz, the inclusion should exhibit a mixture of quartz and coesite at room T, and a P_{inc} at the phase boundary (2.4 GPa). However, if the kinetics of the transition become hindered at low T, then the inclusion P can drop below the phase boundary, to a pressure controlled by the contrast in elastic properties of the composite quartz+coesite inclusion and its host. Interpretation of the remnant inclusion P_{inc} after such a transformation then requires full modelling of the reaction kinetics in addition to the elastic effects (e.g. Perrillat *et al.* 2003). Note that one of the consequences of a single mineral inclusion undergoing a partial transformation during decreasing pressure to a less dense phase, is that the inclusion P_{inc} is maintained above the external P even when it is cracked open, because the inclusion P_{inc} is maintained by further transformation. In the

absence of plastic flow in the host, the only way that the inclusion P_{inc} can drop to the external pressure is by loss of material from the inclusion, which diminishes the mass of material in the inclusion and hence its density and P_{inc} in the fixed volume of the inclusion.

MINERAL INCLUSIONS: INSIGHTS INTO THE GENESIS OF THE HOST

The "bread and butter" of metamorphic petrology has long been the detailed investigation of inclusion-rich porphyroblasts, the most exploited – and often the most aesthetically appealing – including spectacular garnet porphyroblasts in metasediments (Yardley *et al.* 1990; Passchier & Trouw 2005). Inclusions of sillimanite and andalusite in garnets are commonly preserved for the same reason that quartz is preserved in garnets that reach pressures in the coesite stability field; the inclusions are softer than the garnet host, and thus along the prograde path above the entrapment isomeke P_{inc} remains significantly below the external pressure. These mineral inclusions therefore provide direct constraints for the *PT* conditions of host growth, and thus a first-order estimate of the *PT* trajectory, especially when coupled with data on chemical zoning of the host (Thompson *et al.* 1977; Tracy 1978; Krogh 1982). The same methodology has been more recently applied to quartz and coesite inclusions in garnets in UHP metamorphic rocks (e.g. Parkinson, 2000). Another example was recently provided by Barich *et al*. (2014) who investigated rocks from the anatectic sequence of Jubrique (Betic Cordillera, southern Spain). Here, MI occur alongside mineral inclusions of kyanite in garnet cores and with sillimanite in garnet rims (Fig. 3). This assemblage of inclusions immediately constrains partial melting to have occurred during garnet growth, which itself occurred first at high pressure in the stability field of kyanite, and was then followed by a second growth episode at supra-solidus conditions in the sillimanite stability field (Barich *et al.,* 2014). This example shows how the identification of three different types of inclusions in different microstructural positions allows a direct qualitative description of

metamorphic history, without the employment of more sophisticated petrological tools such as geothermobarometry and phase equilibria modelling.

Isotropic Elastic geobarometry

While the simple identification and composition of inclusions trapped during growth of the host phase have long been used to infer *P-T* points along metamorphic paths, the advent of accurate *PVT* equations of state allows the analysis of the elastic evolution of a single-crystal inclusion to be used to constrain the conditions of entrapment, and thus provide an alternative method of barometry (e.g. Ashley *et al*, 2015; Kouketsu *et al.* 2016). This has been variously termed 'piezobarometry' (Adams *et al*., 1975), 'host-inclusion thermobarometry' (e.g. Zhang, 1998), 'QuiG thermobarometry' when applied to quartz in garnet, and 'Thermoba-Raman-try' when specifically involving inclusion measurement by Raman spectroscopy (Kohn, 2014). Inclusion geobarometry does not require thermodynamic equilibrium between the minerals to have existed at the time of inclusion entrapment. In contrast, because elastic equilibration is by definition instantaneous, elastic geobarometry should record the pressure at the moment of entrapment. A comparison of entrapment conditions inferred by elastic geobarometry with growth conditions inferred from the composition of the host offers a unique opportunity to determine the degree of over-stepping during metamorphic reactions (e.g. Spear, 2014; Wolfe & Spear 2017).

The method, as currently applied, consists of measuring the remnant pressure P_{inc} in the inclusion, while the host is at room conditions, by Raman spectroscopy or *in-situ* X-ray diffraction (e.g. Nestola *et al*, 2011). The difference between P_{inc} and room pressure, and the elastic properties of the two phases, is used to calculate ΔP_{relax}, and thus the P_{thermo} (Angel *et al*., 2017a). From P_{thermo} the pressure of the entrapment isomeke at room temperature can be calculated. Then the Equations of State of the host and inclusion can be used to calculate the entrapment isomeke, which represents all *P-T* points at which the inclusion may have been

trapped (e.g. Fig. 1a, b). Note that, because only one quantity, the P_{inc}, is measured on the inclusion, a unique entrapment P and T cannot be determined from this isotropic analysis. An independent determination of either the P or the T of entrapment, for example from classical barometry using phase equilibria, then allows the entrapment conditions to be uniquely determined from the measurement of P_{inc}.

Elastic geobarometry, as currently applied to single-phase inclusions in this way, relies on several assumptions: (1) that the inclusion is spherical and completely fills the hole in the host, both when measured and at the time of entrapment; (2) that the inclusion and host were under the same hydrostatic stress and temperature at the moment of entrapment; and (3) that both phases are elastically isotropic. No mineral is elastically isotropic. However, garnets are almost elastically isotropic and diamonds are so much stiffer than silicates that the effects of their elastic anisotropy on the P_{inc} of spherical inclusions are smaller than measurement uncertainties. As a consequence, the measurement of the P_{inc} of garnet inclusions in diamonds yields calculated entrapment isomekes consistent with independent estimates of the conditions of diamond growth (e.g. Howell *et al*., 2010; Kueter *et al*., 2016).

Problems arising from elastic anisotropy of inclusion minerals are also avoided when mineral inclusions are trapped with a fluid. For example, olivine inclusions in diamonds are normally surrounded by a thin film of aqueous fluid (Nimis *et al.,* 2016), and this ensures hydrostatic conditions for the olivine, much like the pressure fluid in a diamond-anvil cell. The fluid film occupies only a few % of the total volume of the inclusion and its volume expansion will be similar to that of olivine from typical entrapment conditions to ambient conditions if it is dominated by H_2O (Zhang & Duan 2005). The effect of the fluid film on final inclusion pressures is therefore small (Angel *et al*. 2018) and, for estimates of entrapment conditions, can even be ignored, except for the important point that the presence of the fluid allows calculations to use the hydrostatic EoS of the inclusion crystal. Olivine inclusion pressures measured either by Raman spectroscopy (Izraeli *et al*., 1999; Howell *et*

al., 2010) or X-ray diffraction (e.g. Nestola *et al*., 2011) or both (Howell *et al.*, 2012) are then consistent with entrapment at shallow lithospheric mantle depths at temperatures on cratonic geotherms (Angel *et al*. 2018).

Anisotropic Elastic geobarometry

When the isotropic analysis has been applied to quartz inclusions in garnet it can yield systematically incorrect entrapment pressures for some rocks (e.g. Ashley *et al.,* 2016), and an unrealistic spread in values of P_{trap} for quartz inclusions in a single host (e.g. Kouketsu *et al*., 2016; Viete *et al.* 2017). Finite-element modelling shows that some of these problems arise from the inclusions being non-spherical. When the axial ratios of the inclusions significantly exceed 2:1:1, the elastic relaxation is changed, leading to a P_{inc} that differs from that expected for a spherical inclusion entrapped under the same conditions (Mazzucchelli *et al.,* 2018a). Once the effects of shape and other geometric effects, such as proximity to external surfaces and other inclusions, have been allowed for, experimentally-synthesised inclusions measured by Raman spectroscopy exhibit slightly higher P_{inc} than expected from a spherical isotropic model, and the back-calculated entrapment pressures at the synthesis temperatures are typically 0.1-0.2 GPa higher than the pressure of synthesis (Thomas & Spear, 2018). The cause is the elastic anisotropy of the inclusion crystal. A single crystal inclusion in a cubic host crystal such as garnet is subject to uniform strain following a change in P and T from the entrapment conditions; an elastically-anisotropic quartz inclusion must therefore be under anisotropic stress and thus its stress state cannot be characterised by a single "pressure". Deviatoric stresses change the bond lengths and angles in a crystal differently from hydrostatic pressure (e.g. Zhao *et al.,* 2011). The Raman band shifts, which depend on bonding forces within the crystal structure, are therefore different under deviatoric stress than under hydrostatic stress (e.g. Briggs & Ramdas, 1977). Computer simulations of the crystal structure using Density-Functional Theory (DFT) can be used to calculate the shifts of the

Raman peaks of the inclusion under uniform strain and deviatoric stress (Murri *et al*., 2018). These DFT calibrations, in combination with a description of the *P-T* variation of the unit-cell parameters of the inclusion from experimental data (e.g., Angel *et al*., 2014b), can be used for specific host-inclusion pairs to calculate corrections to the P_{trap} calculated from the isotropic model (Alvaro et al., 2018).

Pressure resetting

Some inclusions do not exhibit the residual P_{inc} that is expected, even after allowance for the effects of elastic anisotropy. Sometimes this can be due to phase transformations within the inclusion, as for coesite inverting to quartz. If this can be excluded, the measurement of a P_{inc} that is lower than expected can often be blamed on pressure loss due to cracking (Tajčmanová *et al*., 2014; Angel *et al*., 2015b). Cracking cannot explain the over-pressures measured in micro-diamond inclusions in garnets from Variscan granulites in the Bohemian Massif that were trapped at peak conditions (Kotková *et al.,* 2011) because the measurements imply pressure gain, not loss. Such over-pressures can only be developed in the diamond inclusions if the relevant isomeke puts room conditions into the over-pressure field, which in turn requires that the isomeke is at negative pressures at room temperature (Fig. 1c). This indicates that the inclusion was elastically re-equilibrated (e.g. by plastic flow in the garnet host) at high temperatures and lower pressures in the stability field of graphite (Fig. 1c), consistent also with the observed partial inversion of diamond to graphite in some inclusions. In this case, the elastic analysis of the diamond-in-garnet inclusions using the isomeke concept provides qualitative independent evidence that the Variscan granulites experienced pressure reduction as a result of partial exhumation at high temperatures in agreement with the *P-T* path inferred from conventional petrology (Haifler & Kotková, 2016).

MELT INCLUSIONS AND CRUSTAL ANATEXIS

For more than three decades, the study of crustal differentiation has relied almost exclusively on experiments to identify the melting reactions and melt compositions (e.g. Clemens & Wall, 1981; Vielzeuf & Clemens 1992; Vielzeuf & Montel 1994; Carrington & Harley 1995; Patiño-Douce & Harris 1998; Stevens *et al.,* 1997) and to quantify the evolution of melt properties under different conditions (e.g. Dingwell *et al.,* 1995; Johannes & Holtz 1995; Holtz *et al.,* 2001; Tamic *et al.,* 2001). Melting experiments are a powerful tool, but they can only tell us *what may happen* in Nature for a given starting material under well-constrained conditions. The possibility of obtaining a comprehensive view of crustal melting through experiments is limited by the enormous complexity of the crust itself, and by not knowing the composition of the rock before it melted. To understand precisely what actually happens during anataxis, the natural melt preserved as MI must be targeted (we use the general term 'melt inclusion' to refer to any inclusion that was trapped as melt ±trapped phases). The investigation of natural MI in partially melted rocks (Cesare *et al*. 2009, 2011; Ferrero *et al*., 2012; 2014, 2015, 2016a, b, 2018; Bartoli *et al*., 2013a,b, 2015, 2016; Acosta-Vigil *et al.* 2007, 2010, 2012, 2016) then provides the natural dataset that will enable the extensive "reference frame" from experiments to be used to understand crustal anatexis (Acosta-Vigil *et al.,* 2017).

Any phase recrystallizing in the presence of melt may trap melt droplets, especially under rapid heating conditions and disequilibrium melting (e.g. Cesare *et al*., 1997; Acosta-Vigil *et al*., 2010). Garnet is the most common host for melt inclusions because it is the most widespread peritectic phase generated during incongruent melting in the continental crust (Figs 4a,b,c,d). Much less common hosts of MI in partially melted metamorphic rocks are ilmenite, spinel, cordierite, plagioclase, monazite, zircon, titanite (Figs 4f,g for the last two;

see complete list of hosts in Cesare *et al.,* 2015) and, in a single case study so far, corundum (Palke *et al.* 2017).

Anatectic melt inclusions exhibit varying degrees of crystallization, from fully glassy in rare cases (Cesare *et al*., 2009) to completely crystalline "nanogranitoids" (Cesare *et al*. 2015). Regardless of their crystallization state, in the absence of cracks connecting the inclusion with the rock matrix they can be regarded as preserved and untouched volumes of original melt (Ferrero *et al*., 2016b). The majority of nanogranitoids with sizes ≤10 μm in garnet from high grade terranes shows fully developed negative crystal shapes, i.e. they mimic the shape of the host garnet (Fig. 4b ,c). While negative crystal is the most common shape, tubular shapes have been also observed in nanogranitoids hosted in garnet. For example Darling *et al*. (1997) reported tubular polycrystalline inclusions interpreted as former MI in garnet megacrysts from the Barton Mine, Central Adirondacks, US (Fig. 5a). More extreme examples of polycrystalline needles (Fig. 5b) were recently reported by Axler & Ague (2015) in granulites from the Acadian orogeny, northeastern Connecticut, whose origin as former MI was verified via successful re-homogenization (Ferrero *et al*., 2017; unpublished data).

After re-homogenisation under confining pressure, the composition of the MI allows the chemistry of deep partial melts to be determined directly and completely, including major elements (Acosta *et al*., 2007; Cesare *et al*., 2009; Ferrero *et al*., 2012, 2014; Bartoli *et al*., 2013a,b), trace elements (Acosta-Vigil *et al*. 2010, 2012; Ferrero *et al*., 2018b), and volatiles (Bartoli *et al*., 2014; Acosta-Vigil *et al*., 2016). A dataset of different melts produced via partial melting and trapped as nanogranitoids is already available (Bartoli *et al.,* 2016). It represents the first fundamental step towards a precise identification and quantification of the processes responsible for the generation of S-type granites observed at shallow crustal levels (e.g. Garcia-Arias & Stevens, 2017; for more details see Bartoli *et al.,* 2016).

Recent modelling of melt-phase equilibria using thermodynamic datasets has reproduced the observed compositional trends, but provided only roughly consistent melt compositions (White *et al.,* 2011), because the models rely on an estimated original rock composition as the starting point. However, melt migration commonly results in the preferential removal of some components (Sawyer *et al.,* 2011; Brown, 2013; Yakymchuk & Brown, 2014). Melt-reintegration procedures were first developed to circumvent this problem by White *et al*. (2004), and these have evolved into a routine tool for metamorphic petrologists investigating partially melted rocks (see review by Bartoli, 2017). In contrast, melt preserved in anatectic MI is as close as we can get to the real melt produced at depth, and this melt can now be directly used to reconstruct the original protolith before melt loss. Bartoli (2017) successfully back-calculated both the original protolith and melt productivity of highly residual granulitic enclaves from El Hoyazo, Southern Spain (Fig. 6; see Cesare, 2008 for more details about these rocks), using for the first time the composition of the anatectic MI found in the same rocks. This approach can also be successful even when the partially melted rock does not contain any preserved nanogranitoids, as demonstrated by Bartoli (2018) who used nanogranitoid compositions from rocks with similar protoliths and melted under similar *P*, *T* and H_2O conditions (Bartoli et al. 2016). These results provide a strong argument in support of the use of anatectic MI compositions as a viable approach to model the processes of partial melting and melt extraction.

Melt inclusions are also useful in other ways, for example, they allow the identification of the true genesis of garnets. In medium- to high-grade metamorphic crustal rocks, garnet may form on the prograde path well before partial melting conditions are reached (e.g. Spear, 1993). Thus, the distinction between sub-solidus and supra-solidus garnets may be problematic (e.g. Xia & Zhou, 2017); however, the distinction between the two can be achieved by the identification of primary MI (Cesare *et al.* 2015).

The most common structural evidence for partial melting is the presence of well-defined leucosome domains in the rock, while at the microscale, pseudomorphs after melt filled pores (e.g. Holness & Sawyer, 2008), euhedral crystals and, or, crystal overgrowths formed during melting (peritectic phases) or crystallized from the melt (e.g. feldspar; Vernon, 2011) are often observed. Such evidence can, however, be obliterated as result of melt loss, deformation and extensive chemical re-equilibration during retrogression (Marchildon & Brown, 2006; White *et al.* 2011). In absence of such evidence, MI in refractory phases with large stability fields such as garnet (Baxter & Scherer, 2013) may become the only surviving witness of an anatectic event. One can furthermore use the microstructural constraints provided by anatectic MI to precisely pinpoint the melting event by dating the host and calculating its formation conditions. For example, Walczak *et al*. (2017) performed Lu-Hf dating on garnets for which Ferrero *et al*. (2015) previously reported the presence of melt inclusions, thus constraining the partial melting of the Orlica-Śnieżnik felsic granulites (Bohemian Massif) at 346-348 Ma, while Li *et al*. (2016) dated nanogranitoid-bearing zircons and titanites of anatectic origin from migmatites of the Sulu orogen (China), identifying two distinct melting events.

Because MI in metamorphic rocks have been overlooked for decades, this novel branch of inclusion studies is bound to deliver unexpected findings in addition to constraining the conventional interpretations of crustal anatexis. For example, Ferrero *et al*. (2016a) reported the presence of calcite-bearing polycrystalline inclusions strongly resembling nanogranitoids (Fig. 7) in medium *P* migmatites of the Oberpfalz area, Moldanubian Zone (Bohemian Massif). Microchemical, microstructural and experimental evidence all point to their interpretation as droplets of carbonatitic melt of crustal origin, generated via partial melting at *P-T* conditions much shallower than those postulated for common carbonatitic melts (Ferrero *et al.,* 2016b).

Preserved melt in deeply-subducted crust

Under *HP* and *UHP* conditions, aqueous fluids can contain large amounts of solutes (Ferrando *et al.,* 2005; Scambelluri *et al.,* 2014, Hermann *et al.* 2006; Hermann & Spandler, 2008), including silica, alumina and alkalis (e.g. Malaspina *et al.,* 2006), which are also the major components of anatectic melts. Below the second critical point (as defined by Hermann & Rubatto, 2014), the boundary between these super-silicic fluids and melt *sensu stricto* corresponds to the wet melting curve. As the temperature increases at constant pressure above that point, the fluid gradually changes into a melt (Hermann & Rubatto, 2014). Thus, in *HP/UHP* terranes, real melt inclusions can only be distinguished from crystallized solute-rich fluids by their mineral assemblage and H_2O content. Nanogranitoids will comprise an assemblage consistent with the crystallization of an H_2O-bearing melt, i.e. quartz, feldspars, one or more OH-bearing phases and maybe an H_2O-filled porosity (Fig. 8a,b,c,d; see e.g. Ferrero *et al.* 2015). Former solute-rich fluid inclusions (also called multiphase solid inclusions or MSI, Frezzotti & Ferrando 2015) will instead contain mainly OH-bearing phases, e.g. amphibole, chlorite, phlogopite (Fig. 8e,f; Frezzotti & Ferrando, 2015; Malaspina *et al.,* 2006, 2015).

Significant amounts of H_2O are expected to occur in MSI, but they are only rarely preserved (e.g. Malaspina *et al.,* 2017 and below). In the most recent literature, inclusions containing an assemblage consistent with the crystallization of a silicate-rich melt were also reported in garnet and clinopyroxene from different *UHP* crustal terranes (for a comprehensive review see Gao *et al*. (2017)). For descriptive purposes, such inclusions are also generally referred to as MSI, but the presence of quartz ±feldspar(s) and one or more OH-bearing phases would make them more appropriately called nanogranitoids. Beautiful examples of *UHP* MSI inclusions, which are identical to lower-*P* nanogranitoids, are given in Liu *et al*. (2013) and Stepanov *et al*. (2016), e.g., compare Fig. 4b,c,d with Fig. 8b,d.

In some cases, OH-bearing phases are absent and the only remaining evidence for the former presence of volatiles is provided by rounded voids preserved in the inclusions (Gao *et al.,* 2017). As for lower-*P* nanogranitoids, re-homogenization under pressure in the piston cylinder is the most direct way to prove that these *HP/UHP* inclusions were melt droplets at the moment of entrapment, see e.g., Ferrero *et al*. (2015) and Stepanov *et al*. (2016). However, this approach requires that the inclusions are preserved, i.e. they did not undergo decrepitation and material loss. Unfortunately, extensive decrepitation cracks around *HP/UHP* multiphase inclusions are common (see e.g. Gao *et al.,* 2013; Frezzotti & Ferrando, 2015), and this is expected to have caused fluid and, or, material loss as well as chemical re-equilibration with the matrix, thus preventing complete re-homogenization on re-heating (Ferrero *et al.,* 2012).

Besides the experimental approach, the most direct evidence that *HP/UHP* inclusions originally contained melt is provided by the presence of glassy inclusions (Borghini *et al.,* 2017) and, or, residual glass, as is the case for near-*UHP* nanogranitoids from the Bohemian Massif (Ferrero *et al*. 2015, 2016), in which glass was identified via Raman mapping (Fig. 9). Previously, residual glass has been identified using transmitted electron microscopy of multiphase inclusions in microdiamond from the Kokchetav Massif (Hwang *et al.,* 2004; 2006) and in the Erzgebirge (Hwang *et al.,* 2006), and interpreted as evidence that deep melts play a role in the formation of microdiamonds in subducted crust.

UNDERSTANDING THE MESSAGE OF MI

Metastable phenomena in small containers?

While inclusions remain isolated, their behaviour is expected to be independent from what happens in the surrounding environment. This condition, coupled with the small size of the inclusions, may favor the formation and preservation of phases well outside their stability

field. It is important to note, however, that the independence of the inclusions from the surrounding environment does not make them intrinsically metastable; as we have shown for mineral inclusions, many examples that appear to be metastable are simply exhibiting the stable behavior of an enclosed system under its own peculiar stress state. On the other hand, examples of real metastable behaviour in fluid inclusions have been extensively reported, e.g., the failure of vapour bubbles and, or, ice to nucleate on cooling (Roedder, 1967; Bakker & Baumgartner, 2012; Qiu *et al.* 2016) or the growth of graphite in COH fluid inclusions, apparently triggered by the Raman laser beam (Kerkhof *et al*., 1991), as well evidence of delayed crystallisation of daughter minerals in igneous MI (Roedder, 1971).

Glass

Silicate glass is metastable with respect to crystallisation in an open system at all *P* and *T*. Glass is common in rapidly-cooled MI, but it is also found even in cases with a very slow cooling rate, e.g. 8°C/Myr for the nanogranitoid-bearing Khondalites of Southern India (Cesare *et al.,* 2009). Fully-glassy and partially-crystallized inclusions may coexist with fully crystallized nanogranitoids, despite all containing the same melt and having experienced the same post-entrapment evolution (Ferrero *et al.,* 2012).

Residual glass occurs in nanogranitoids trapped under extremely variable conditions from medium-low *P* (Ferrero *et al.,* 2014; Bartoli *et al.,* 2016 a,b) to near-*UHP* conditions (see Fig. 6; Ferrero *et al.,* 2015, 2016). Clearly, the *PT* conditions of entrapment and subsequent rock history are not the primary control of whether or not glass is preserved and, since the thermodynamics of the inclusion are not size-dependent, the glass must be metastable. It is well known that nucleation is inhibited in small pores (Muncill & Lasaga, 1987; Putnis *et al*., 1995; Holness & Sawyer, 2008; Cesare *et al.,* 2009), and glassy inclusions are generally smaller than co-existing nanogranitoids (Cesare *et al*., 2009), although

exceptions are observed. Bartoli *et al*. (2013), for instance, report several cases of large glassy inclusions coexisting with significantly smaller, fully crystallized, inclusions.

(K, Na)$AlSi_3O_8$ polymorphs

Glass is not the only metastable phase observed in nanogranitoids. Ferrero *et al.* (2016) reported the occurrence of a hexagonal polymorph of $KAlSi_3O_8$, kokchetavite (first reported by Hwang *et al.,* 2004), and an orthorhombic polymorph of $NaAlSi_3O_8$, kumdykolite (Hwang *et al.,* 2009), in nanogranitoids (Fig. 10a). The polymorphs are interpreted as crystallization products of the melt trapped in the inclusions, as these nanogranitoids can be successfully re-homogenized (Ferrero *et al.,* 2015; see also Borghini *et al.,* 2017). Because these phases crystallize in the stability field of their more common counterparts, albite and K-feldspar (Ferrero *et al.,* 2016), they are likely metastable in an open system. Their value is that their presence can then be used as evidence that the inclusions are unaltered MI, as they occur only in inclusions without evidence of decrepitation (Ferrero *et al.,* 2016). Initially, kumdykolite and kokchetavite were reported only in diamond-bearing rocks (Hwang *et al.,* 2004; 2009; Kotková *et al.,* 2014) and in meteorites (Nemeth *et al.,* 2013), suggesting that these phases may be indicative of high, or even ultra-high pressure, although Nemeth *et al.* (2013) recognised that their low density precludes them from being stable at high pressures. The apparent link drawn previously between extreme pressures and the occurrence of these polymorphs was, instead, the result of the strong bias in the available database towards studies targeting *HP* and *UHP* polycrystalline inclusions. Indeed, as the number of studies of nanogranitoids is increasing, with many more lower-*P* occurrences, the metastable feldspar polymorphs are increasingly recognized as a common component of pristine nanogranitoids, regardless of the formation conditions or the bulk rock chemistry.

One or both feldspar polymorphs have been identified in inclusions in garnet from diamond-bearing rocks from the Kokchetav Massif and Bohemian Massif (Hwang *et al.,*

2004; 2009; Kotkova *et al.,* 2014; Perraki & Faryad, 2014), in zircons in *UHP* rocks from the Sulu orogen (J. Liu pers.com.; see also Liu *et al.,* 2015), in *HP* felsic granulites from the Polish Sudetes (Ferrero *et al.,* 2016a) and Gory Sowie (Slupsky *et al*., 2018), in *HP* (ultra)mafic rocks from Granulitgebirge (Borghini *et al.,* 2017) and Antarctica (Ferrero *et al.*, 2018a), in low *P* garnet xenocrysts of the La Galite archipelago, Tunisia (here reported for the first time), and in amphibole from mantle xenoliths of the Rio Grande Rift (Berkesi *et al.,* 2016). Ferrero *et al*. (2016) calculated the *PT* path followed by nanogranitoid inclusions within garnets in *HP* felsic granulites to define the *PT* conditions of formation of the polymorphs, and showed that these phases formed at P_{inc} <<2 GPa (Fig. 10c) in the stability field of albite and K-feldspar. Finally, their occurrence in inclusions trapped at 0.4-0.5 GPa in the La Galite garnet xenocrysts (Fig. 11; see also Ferrero *et al.,* 2014) provides clear proof that these polymorphs can form under any pressure, within the stability fields of the common feldspar minerals.

Within anatectic MI, kumdykolite and kokchetavite crystallize from melt, so in this case they are certainly igneous, rather than metamorphic, phases. However, these polymorphs have never been reported in natural magmatic rocks, so they seem to crystallize preferentially in confined spaces such as inclusions. The previously mentioned inhibition of nucleation in small pores results in undercooled melts when *T* drops below the solidus (e.g. Lofgren, 1974), a condition which has been recognized to promote rapid crystallization once the process starts (Sirbescu *et al.,* 2016; Sirbescu *et al.,* 2017), with quartz expected to grow in a few hours or days, depending on the inclusion size (M. Sirbescu pers. comm.). Metastable phases can then form simply as a result of kinetic preference if their crystal structures more closely resemble the local atomic structure of the melt (Huang & Kieffer, 2004; Kotková *et al*., 2014 and references therein). Of course, the easiest way to achieve melt undercooling and trigger rapid crystallization would be to rapidly cool the host rock, and rapid cooling has already been proposed as an influential factor for the formation of kumdykolite by Hwang *et al*. (2009).

Interestingly, rapid (almost instantaneous) crystallization is consistent with the limited observations available on the formation of Ca-rich kumdykolite, i.e., svyatoslavite (Cheskonov *et al.,* 1989; Abe & Sunagawa, 1995) and kokchetavite (Kanzaki *et al.,* 2012). However, it is difficult to imagine how the natural process of exhumation of deeply subducted rocks can cause instantaneous cooling of the host rocks.

In summary, the available data are consistent with the hypothesis that these polymorphs form as result of rapid *crystallization* of a melt, which is *not caused by rapid cooling* but by the peculiar undercooled and supersaturated conditions achieved on cooling by a melt confined in a small cavity, perhaps further enhanced by the availability of the host mineral surface to act as nucleation sites. Metastable growth as result of the small size of the inclusions was also recently proposed to explain the unexpected coexistence of corundum and quartz in inclusions from the felsic gneisses of the Athabasca Granulite Terrane reported by Tacchetto *et al.* (2018). Other suggestions, for example that the presence of kokchetavite is an indicator of a metasedimentary protolith (Mikhno *et al.,* 2017), is not consistent with the observation that the crystallization products of MI depend exclusively on the chemistry of the trapped melt and are not an inherited feature of the original protolith; kokchetavite has been reported in nanogranitoids from metagranitoids (Ferrero *et al.,* 2016; Figs. 8a, 10a), mafic (Borghini *et al.,* 2017) and ultramafic rocks (Ferrero *et al.,* 2018a).

SiO_2 polymorphs

Cristobalite is another polymorph recognized in nanogranitoids (Fig. 10a) as well as in mineral inclusions in metamorphic rocks. In metamorphic rocks cristobalite was first identified within polycrystalline inclusions, which are possibly former melt or solute-rich fluid, in garnets of the Gore Mountains in the Adirondacks, US (Darling *et al.,* 1997), and, a few years later, in omphacites of the Kokchetav Massif (Hwang *et al.,* 2004), where it often coexists with kokchetavite. More recently, cristobalite was recognized in nanogranitoids from

felsic granulites from both the Bohemian Massif (Ferrero *et al.,* 2016) and the Acadian orogen in Connecticut (Ferrero *et al.,* 2017; see also Ague & Axler (2015) for *P-T* formation conditions). Cristobalite was reported as mineral inclusions in medium *P* garnets by Ashley *et al*. (2015), who proposed it to be the result of post-entrapment transformation under-pressurization of former quartz inclusions. Interestingly, this finding comes from the Adirondacks Highlands, where cristobalite was first reported in garnet by Darling *et al*. (1997).

The most intriguing feature shared by all of these case studies is that none of the host rocks experienced the extreme conditions at which cristobalite is thermodynamically stable, i.e. T >1470 °C and P < 0.2 GPa (Heaney, 1994), thus suggesting its crystallization as a metastable phase. Cristobalite was previously observed to crystallize in the tridymite field (Schairer & Bowen 1956), and thus Darling *et al*. (1997) proposed that OH loss from the polycrystalline inclusions may have lowered the P_{inc} of the inclusion, still at high T conditions, thus bringing the inclusions into the stability field of tridymite, at $T \leq 900$°C. This mechanism cannot, however, be invoked for the nucleation of cristobalite in the near-*UHP* nanogranitoids of the Bohemian Massif, as they show no evidence of H_2O loss (Ferrero *et al.,* 2015). In this example, cristobalite coexists with residual glass, indicating direct crystallization from the melt at T much lower than 875°C (Ferrero *et al.,* 2016), also favoured by the similarities between the structure of cristobalite and the melt (e.g. Huang & Kieffer, 2004). In summary, the available experimental evidence and observations on natural inclusions support the idea that the presence of metastable polymorphs of SiO_2 in inclusions is the result of rapid melt crystallisation in a confined volume.

Thermodynamics of MI

It is important to consider the thermodynamics of MI to investigate whether the preservation of glass or apparently metastable polymorphs could actually represent *stable* behaviour when

viewed from the perspective of the closed system. The thermodynamic situation in a melt inclusion, immediately following entrapment, is similar to that of a mineral inclusion that is softer than its host, because melts will always have a lower bulk modulus than a mineral host (i.e. $\frac{K_{inc}}{K_{host}} < 1$). Thus the pressure inside a MI will remain between the isomeke *P* and the external *P* in the rock applied to the host (e.g., Fig. 12). If the external pressure falls below the entrapment isomeke, the melt inclusion then becomes over-pressurised, causing decrepitation (e.g. Tait 1992; Touret, 2009; Ferrero *et al.,* 2011, 2016).

The glass transition does not result in a volume change, although there is a small reduction in the thermal expansion and compressibility of the inclusion (e.g. Knoche *et al.*, 1992), which reduces the contrast between the elastic properties of host and inclusion. Vitrification therefore leads to no sudden pressure change in the inclusion, but only a deflection in the P_{inc} path so as to reduce the difference from the external pressure. In contrast, crystallisation generally produces a significant density increase of several %, so partial or complete crystallisation of thermodynamically stable phases will typically produce a sharp pressure drop in the inclusion. This is exactly the reverse effect to that of melting discussed above, and crystallisation of the inclusion will be energetically favoured while the inclusion is over-pressured with respect to the external pressure, e.g. along a classic clock-wise *PT* path where cooling is associated with decompression (Fig 12). For such exhumation paths, glass preservation is therefore confirmed as a consequence of metastability.

There is a theoretical possibility that polymorphs found in MI are actually thermodynamically stable: this would occur if the external *P-T* path crosses the entrapment isomeke to the high-pressure side, thus rendering the MI under-pressured with respect to the outside (Fig. 12). Under these conditions, the pressure in the inclusion can be increased, and thus *P* gradients in the system reduced (equivalent to reducing the free energy) by crystallising phases less dense than the melt. Although the atmospheric pressure densities of

the metastable polymorphs of feldspars are lower than those of the corresponding stable phases by about 4-5% (e.g. Nemeth et al., 2013) their thermal equations of state, and hence their densities at metamorphic *P* and *T*, are unknown. Nonetheless, it is reasonable to assume that the metastable polymorphs remain less dense than the stable feldspars at high *P* and *T*, otherwise they would become the stable phases.

Using albite compositions with EoS from Thermocalc (Holland & Powell, 2011) as an example, at liquidus *P* and *T* the density of the melt approaches within 5% of that of albite crystals at pressures above 2.5 GPa. Under these conditions it is quite likely that the density of the metastable kumdykolite becomes equal to, or less than, that of the melt. If this is really the case, the key question relating to the thermodynamic stabilisation of "metastable" phases in the inclusions becomes "How can the cooling path (external *P* and *T*) cross the entrapment isomeke so that the external *P* and *T* are above the isomeke?". The answer to this depends on the conditions under which the MI were entrapped, coupled with the *P-T* path followed by the host rock after the MI formation.

Melt-garnet isomekes differ from those for crystalline inclusions because the thermal expansion coefficients of melts are typically much higher than those of the host, whereas the melt bulk modulus does not differ by a large amount from the corresponding crystals. Therefore, the slopes of melt-inclusion isomekes with host crystals like garnets are far steeper, e.g., 1 – 8 GPa/1000 °C, than for crystalline inclusions, and the slope increases significantly with increasing pressure as a consequence of the strong decrease in the thermal expansion coefficient of melts with increasing pressure (Fig. 13). While for MI trapped at shallow depths (e.g., in the garnets of magmatic enclaves in granodiorites; Ferrero et al., 2014) there is only limited de-pressurisation of the rocks by 0.2-0.3 GPa, and the relatively shallow slope of the isomekes means that significant subsequent cooling (Fig. 13a) is required to take the inclusion back across the entrapment isomeke into the regime where the crystallisation of low-density polymorphs is thermodynamically preferred over the more dense 'stable' phases. The

significant cooling required for crossing the entrapment isomeke before crystallization would also cause the confined melt to achieve the undercooled and supersaturated conditions which we suggested were the major factors likely to promote formation of metastable polymorphs.

For MI trapped under *HP* and *UHP* conditions, the isomekes are steeper and the required isobaric cooling required to take the inclusion into the under-pressure field is less (Fig 13b). The problem, however, is that exhumation paths are initially approximately isothermal, so that the inclusion pressure also drops a long way below the entrapment isomeke, and no amount of subsequent isobaric cooling can take it back across the entrapment isomeke (Fig. 13b). A third possibility is that the stress field developed in the host around the inclusion, as a result of decompression and the resulting contrast between the inclusion pressure P_{inc} and the external pressure P_{ext}, will drive plastic flow and, given enough time or temperature, will result in the inclusion pressure being reset equal to the prevailing external pressure via stretching of the inclusions (e.g. discussion in Stöckhert *et al.* (2009)). The timescales for such resetting are uncertain because of uncertainties in extrapolating experimental data from laboratory to geological timescales (e.g. Dabrowski *et al.,* 2015; Zhong et al., 2018). It is, however, clear from the example provided by the diamonds in Variscan garnets (Kotkova *et al.,* 2011), discussed above, that plastic flow in garnet is sufficiently rapid above 900-1000 °C to completely reset the inclusion stress during exhumation. For a MI in a garnet, this would reset the relevant isomeke (Fig. 13b). However, because melt-garnet isomekes become shallower at lower pressures, the rock cooling paths still do not then return to cross the reset isomeke. What would be required to stabilise metastable phases is that the isomeke is reset *and* is then crossed by what is required to be close-to-isobaric cooling: these conditions may be achieved in natural rocks, for example through reheating of deeply subducted rocks after partial exhumation (Fig. 13c).

Lower *P* reheating after a high *P* event has been proposed for many rocks in *UHP* terranes; for example, as result of under-plating in the Bohemian Massif (O´Brien *et al.,* 2001)

or post-exhumation thermal relaxation in the Himalaya (Wilke *et al.,* 2015). This has known effects on the geochemistry of the mineral phases, including the resetting of compositional profiles across garnets (e.g. O´Brien, 1997) and, if diffusion is rapid in the garnet, clearly plastic flow can also occur. In this sense, it is therefore possible that the appearance of metastable phases preserved in former MI is not only an indicator of them remaining pristine and unbroken, but may also be a consequence of thermodynamically stable behaviour after isomeke resetting. Clearly resolving such a question requires more detailed data on the phases occurring in MI and to determine whether they are correlated with the *PT* paths of the host rocks.

Preserved volatiles in deep melt and fluid inclusions

The presence of metastable phases supports the idea that inclusions can behave as closed thermodynamic systems and thus remain fully preserved during the whole post-entrapment history of their host. However, several case studies of fluid inclusions in HP/UHP metamorphic rocks show evidence of H_2O loss during exhumation and depressurization, commonly visible as decrepitation cracks (e.g. Frezzotti & Ferrando, 2015). In some cases, such cracks are partially healed into trails of sub-micrometric fluid inclusions, and only TEM observation can prove their existence (Vityk *et al.,* 2000; Viti & Frezzotti, 2001; Ferrero *et al.,* 2011). H_2O loss can also occur via diffusion of hydrous components from the inclusion to the matrix through the host (Frezzotti *et al.,* 2012; Frezzotti & Ferrando, 2015), a phenomenon also supported by experiments on garnet (Wang *et al.,* 1996).

Recent studies support the idea that inclusions in *UHP* rocks may instead preserve a H_2O content consistent with their formation conditions. For instance Malaspina *et al*. (2017) recently reported large amounts of preserved H_2O detected via FTIR mapping (Fig. 14) in multiphase inclusions from *UHP* garnet orthopyroxenites of the Maowu Ultramafic Complex, China. These rocks equilibrated at 4 GPa and 750-800°C (see also Malaspina *et al.,* 2006) and

the inclusions, hosted in garnet, are the result of the crystallization of a supercritical aqueous fluid. The presence of H_2O suggests that these inclusions still behave as a locally closed system (Malaspina *et al.,* 2017). The same also appears to be true for melt droplets originally trapped near the *HP/UHP* transition: nanogranitoids from the Polish Sudetes still contain their original H_2O content, as verified via Raman investigation (Ferrero *et al.,* 2015) and nanoSIMS measurement (Ferrero *et al.,* 2016 and unpublished data) after re-homogenization. These inclusions in fact contain 6.2 wt % of H_2O (measured via NanoSIMS; Fig. 14b) after re-homogenization, an amount consistent with that observed in experimental melts (Hermann & Spandler, 2008) formed under similar *P-T* conditions (~900°C and 2.7 GPa; see also discussion in Ferrero *et al.,* 2015). No H_2O transfer seems to have occurred during cooling and exhumation from these tiny volumes of melt, and no cracks are visible connecting the inclusions with the host matrix (Ferrero *et al.,* 2016). That re-homogenized nanogranitoids maintain their pristine H_2O content was already proven in low *P* inclusions after a detailed NanoSIMS investigation by Bartoli *et al*. (2014).

Further support for this idea is provided by the fact that we can completely re-homogenize these inclusions at the formation conditions of the garnet (Ferrero *et al.,* 2015). Any H_2O loss would move the liquidus to higher temperatures (Johannes & Holtz, 1996) and thus cause the nanogranitoids to melt at higher temperatures, inconsistent with the results of independent geobarometric and thermodynamic calculations (Cesare *et al.,* 2015). H^+ loss through the garnet would be as easily detectable in the experimental products of re-homogenization experiments of nanogranitoids. Such loss would cause the persistence of a shrinkage bubble on re-homogenization due to the loss of material, and thus incomplete re-homogenization. Moreover, H^+ loss would cause excess oxygen to be present in the MI, and as this tiny volume of melt is generally enclosed by a Fe-rich host (i.e. the garnet), an iron oxide would form under re-heating, as reported by Danyushevsky *et al*. (2002) for magmatic MI hosted in Fe-bearing olivine. For more details about the problems of H_2O loss/gain in

nanogranitoids see the discussion in Bartoli *et al*. (2014). In summary, despite the high mobility of H_2O in metamorphic environments, inclusions of partial melt as well as (some) fluid inclusions seem to preserve their original H_2O content, even when these inclusions formed under extreme conditions in deeply subducted rocks.

PERSPECTIVES

The field of study of inclusions in minerals is undergoing rapid development, and further research avenues are likely to open, enabling us to target novel aspects of the "inclusions in minerals" field of research. In which directions is this field heading, and which are the most fruitful avenues of research that should be exploited in the future?

Testing the origin of the inclusions

A secure identification of the origin of the mineral inclusion visible in metamorphic minerals is still a daunting task, representing a priority for the future development of the field. Mineral inclusions in metamorphic minerals can be either leftover reactants or products of the chemical reaction responsible for the host formation, or phases which did not participate in these reactions (Yardley et al., 1991) - those which Passchier & Trouw (2005) refer to as "passive inclusions". Further complications are posed by the presence, especially in minerals formed under high temperature/pressure conditions, of mineral inclusions that are instead the result of later modifications of the host itself, i.e. exsolution products, with or without exchange of material with the surrounding matrix. In metamorphic rocks, the most common occurrence is probably represented by rutile ± ilmenite needles in garnet (e.g. Proyer *et al.,* 2013; Axler & Ague, 2015 and references therein).

One possible method to constrain the origin of inclusions is to determine their crystallographic orientation relationships (CORs) to their host crystals (Griffiths *et al.,* 2016),

although the concept of a COR is strictly descriptive and what this may indicate for the genesis of the inclusion is a matter of interpretation. A common well-defined orientation of inclusions with respect to their hosts has long been used to argue for an exsolution origin. During solid-state exsolution, the exsolved phase is often structurally related to the host and thus the controlling factors on inclusion orientation and morphology is the interfacial energy, particularly the coherency strain (Williame & Brown, 1974). Examples of such orientation control are provided by exsolution lamellae of Ca-poor pyroxene from augite, and *vice versa*, whose orientation can be used as a geothermometer (Robinson *et al.,* 1977), and the perthitic microstructures in alkali feldspars whose orientation and scale can be used as a geospeedometer (Parsons *et al.,* 2015). Other types of CORs might be expected to form when inclusions are trapped by, rather than exsolved from, the host. If the inclusions are remnant fragments of the protolith, one might expect a completely random orientation of the inclusions relative to the host minerals. On the other hand, if the inclusion is a product of the host-forming reaction it may well have nucleated and grown on the existing host crystal, in which case some non-random COR may be expected. In the latter scenario, if the nucleation and subsequent growth is epitaxial, a specific single COR will be exhibited by the inclusions. If the individual surface energies are the dominant control, one might expect that the COR exhibits parallelism of one crystallographic inclusion face to one of the host, but without preferred orientation in the plane of the common faces. This has been termed a 'rotational' COR and is found in several types of inclusions in garnets (Fig. 15).

A recent key observation is that, even for a single inclusion mineral within a single garnet, there are often several different populations of inclusions represented by different CORs (Fig. 15). The correct interpretation of CORs must therefore rely on statistical analysis of large numbers of inclusion orientations in many host crystals. This is now possible with semi-automated high-resolution EBSD measurements, associated indexing algorithms in software, and the appropriate handling of crystallographic symmetry (Angel *et al*., 2015a;

Griffiths *et al*., 2016) without which the COR will appear more random than it really is. For example, obtaining sufficient measurements for statistical assessment of CORs was the key to using olivine orientations in diamonds to constrain the mechanism of diamond growth in the cratonic lithosphere. Prior to recent measurements, there was simply insufficient numbers of data to determine whether olivine inclusions in diamonds exhibited a specific crystallographic preferred orientation, a specific COR, relative to their diamond hosts. This allowed various hypotheses about diamond growth and, in particular, the relationship between the age of inclusions and the age of diamond formation, to be entertained (e.g. Sobolev, 1977; Taylor *et al.*, 2003). The recent measurement of the CORs between a large number of olivine inclusions and their diamond hosts has resolved these questions. Olivine inclusions in different diamonds from different localities (Nestola *et al*., 2014; Neusser *et al.*, 2015; Milani *et al,*. 2016, and references therein) are, overall, randomly oriented with respect to their diamond hosts. This indicates that there is no interfacial control on the olivine orientations, hardly surprising in the light of the subsequent discovery of ubiquitous hydrous fluid films surrounding olivine and other silicate inclusions in diamond (Nimis *et al.,* 2016). The fact that olivines in the same diamond frequently share a common crystallographic orientation, independent of their orientation with respect to the diamond, can then only be explained if the iso-oriented inclusions are the remnant fragments of olivine single crystals in the host rocks within which the diamonds grew, while pre-existing olivine grains were dissolved by a fluid. Thus, the olivine inclusions cannot be the product of the diamond-forming reaction, eliminating reactions of the type orthopyroxene + carbonate = olivine + diamond + O_2 as being responsible for diamond formation. Instead, the measured CORs of olivines to their host diamonds confirm the interpretation from geochemistry (e.g. Luth & Stachel, 2014; Stachel & Luth, 2015) that cratonic diamonds are precipitated directly from COH fluids/melts while the fluid simultaneously corrodes the pre-existing minerals. This conclusion is supported by the observation of a different type of COR of chromite inclusions in diamonds which is not as

random as olivines, but is 'rotational' with one of the {111} faces of the chromite being sub-parallel to a {111} face of the diamond (Alvaro *et al*., 2017). This arises from the dominant morphologies of spinel and diamond which will occur in the presence of a fluid that will dissolve higher-energy surfaces. Olivine does not display such morphological control because the variation of surface energy with face orientation is much smaller (Bruno *et al*., 2014), as is obvious from its more complex common morphology.

The number of measurements of CORs in metamorphic minerals with sufficient statistics remains very limited, but the available data already suggest that petrological information is encoded in COR distributions. For example, the variations in COR frequencies between samples appears to correlate with the conditions and mechanisms of development of the host-inclusion system, with the highest-temperature systems showing a lower diversity of CORs (Griffiths *et al.,* 2017). Testing the potential of this idea requires much more data to be collected from a variety of host/inclusion systems in different geological settings: a fundamental understanding of the various factors leading to CORs also needs to be developed.

High resolution characterization of the inclusions

Inclusions are generally very small, in some case just few μm, and their size poses the greatest challenge: however, the spatial resolution of the most modern analytical techniques is rapidly improving. For example, we can now routinely probe, and obtain quantitative information from, micron- and submicron-sized inclusions through various *in situ* analytical techniques. The increasingly easier access to high computational power makes it less burdensome to analyse these data and incorporate them into thermodynamic and physical models.

As smaller and smaller portions of mineral inclusions, MI and FI are investigated, they appear to be more and more inhomogeneous. Such inhomogeneity needs to be investigated, and its causes understood and quantified. This task is already being pursued: the latest generation of electron microprobes equipped with Field Emission Guns, recent LA-ICP-MS

systems, Transmission Electron Microscopy, synchrotron-based techniques and NanoSIMS already provide reliable geochemical data on volumes of material down to a few cubic microns. *In situ* X-ray diffraction is a powerful tool to investigate the mutual relationships between inclusions and, or, polycrystalline aggregates a few microns in size, and their host. For example, Malaspina *et al.* (2015) recently applied for the first time this technique to polycrystalline inclusions hosted in UHP rocks, originally containing super-silicic fluid, to identify epitaxial growth and preferred crystallographic orientation of the phases in the inclusions. The same technique is also ideal for investigations of crystallization in small volumes, e.g. near-equilibrium versus far-from-equilibrium crystallization of mineral phases and dissolution re-precipitation of the host (Malaspina *et al.,* 2015).

3D microtomography of μm and sub-μm single fluid inclusions via X-ray fluorescence has been performed for more than a decade (e.g. Menez, 2001; Rickers *et al.,* 2004), and the combination of Focused Ion Beam (FIB) preparation of samples with SEM observations is increasingly becoming a routine, yet still time-intensive, approach (Wirth, 2009; see also Tacchetto *et al*., 2018 and Cesare *et al.* 2015 for its first application to nanogranitoids). Technological developments are increasingly allowing us to couple sub-micron analyses with investigation of larger volumes of material. As a result, 3D high resolution tomography has acquired an increasing importance in micropetrology, e.g., for mineral inclusions in garnet porphyroblasts (e.g. Huddlestone-Holmes & Ketcham, 2005, 2010; Moore & Carlson, 2015) and in diamonds (Nestola *et al.,* 2012), glass inclusions in magmatic quartz (e.g. Gualda & Rivers, 2006; Pamucku *et al.*, 2013), fluid inclusions in metamorphic rocks (e.g. Yoshida *et al.,* 2016). More recently, Parisatto *et al.* (2018) applied this technique to the investigation of the distribution of primary MI in peritectic garnet. These new results on the size, shape and distribution of the inclusions provide direct constraints for the identification and quantification of the factors influencing crystal growth processes and inclusion formation,

thus providing the data necessary for the interpretation of a wide range of both magmatic and metamorphic processes.

Experimental petrology to solve inclusion-related problems

Experimental petrology offers the possibility of reproducing natural processes under controlled laboratory conditions, leading to the quantification of the intensive variables influencing natural processes. This approach holds the key to the future creation of a rigorous systematic treatment of inclusion formation and interpretation based on the production of synthetic inclusions.

The synthetic inclusion approach has been widely applied to the investigation of FI and MI in subsolidus and igneous systems since the early 80s (e.g. Sterner & Bodnar, 1984; Schmidt *et al.,* 1998; Student & Bodnar, 1999; Lecumberri-Sanchez *et al.,* 2015; Steele-McInnis *et al.,* 2015). Inclusions were synthesized by healing fractures in quartz in the presence of fluid and, or, melt under known *P-T-X* fluid conditions (Bodnar, 1989). As FI and MI can be produced under conditions identical to the natural ones, the properties of various fluid systems can be quantified over an extended range of geologically significant conditions (Bodnar, 1989). However, the method has only been applied to quartz as this phase is one of the most common host minerals for FI and MI, and its simple composition makes it relatively easy to work with. The application of the synthetic inclusion approach to less conventional hosts would provide the constraints necessary to interpret FI and MI in a wider range of environments and *P-T-X* conditions. Garnet, as a widespread host of MI and mineral inclusions, would be an ideal target for a dedicated experimental campaign aimed at creating synthetic inclusions. Garnet formation is not only commonly documented in melting experiments on crustal compositions (Vielzeuf & Montel, 1994; Carrington & Harley, 1995; Auzeanneau *et al.,* 2006; Hermann & Spandler, 2008), but melting experiments have also produced peritectic garnet with demonstrable MI (Gardien *et al.,* 1995; P. Tropper, pers.

comm.; G. Stevens, pers. comm., see also Laurie & Stevens, 2012), and some garnets have been grown to trap solid inclusions (e.g. Spear et al., 2014, Thomas and Spear, 2018). Furthermore, synthetic inclusions in garnet could be used to identify and quantify the factors controlling the preservation of glass or the formation of polymorphs in nanogranitoids, e.g., by subjecting them to heating/cooling and compression/decompression cycles at variable rates, to simulate *P-T* variations experienced during metamorphism, as well as to monitor shape changes as a function of *T* and *t*.

Elastic geobarometry

We have discussed in qualitative terms the process of resetting the inclusion pressure P_{inc} as a result of plastic flow in the host mineral. This is driven by the stress gradient set up in the host, because P_{inc} differs from the external pressure as soon as the rock *PT* path leaves the entrapment isomeke. Therefore, as we have discussed in the context of our examples, at temperatures sufficiently high to allow plastic flow, the actual P_{inc} lies somewhere between the value expected for purely elastic behaviour and the external pressure. Recently, Zhong *et al.* (2018) have shown that the timescales for this loss in P_{inc} can be calculated for isotropic spherical inclusions in a visco-elastic model, using plastic flow laws derived from experimental data. Inverting the analysis, they also demonstrate that P_{inc} values measured in the recovered rocks can be used to provide estimates of cooling timescales that are in agreement with conventional methods for rocks ranging from eclogites to kimberlites (Zhong *et al.*, 2018). This kind of modelling, while requiring refinement to include the effects of anisotropy of shapes and elasticity, and significant improvement in the precision of laboratory determinations of plastic flow laws and their dependence on pressure, offers the possibility for providing for the first time precise constraints on cooling rates based on microstructural observations and measurements from a purely mechanical perspective.

Anisotropic inclusion phases, such as quartz, represent both a challenge and an opportunity for performing piezo-barometry. As we have described above, the current theory for elastic geobarometry is only developed for elastically isotropic systems with the ideal geometry of an isolated spherical inclusion and, when applied in combination with hydrostatic calibrations of Raman shifts, can yield systematically wrong entrapment pressures. Modern computing power allows finite-element elastic models to be used to calculate explicitly the mutual relaxation step, which depends strongly on the interaction of shape and elastic anisotropy (Mazzucchelli *et al*., 2018a, b), and provide maps of corrections to the P_{trap} inferred from the isotropic models and calibrations, at least for quartz (Alvaro *et al*., 2018).

What is also clear is that measuring the shift of a single Raman band of an anisotropic inclusion mineral such as quartz does not allow the true anisotropic stress state of the inclusion to be determined. A generalisation of the Raman method using the Grünesien tensor allows the full strain state of an inclusion to be measured (Murri *et al*., 2018), which opens the intriguing opportunity to measure the deviatoric stress state in inclusions and interpret it in terms of the stress field in the rock at the time of entrapment. Inclusions, in brief, may be able to provide not only unique information about the palaeo-chemistry of a rock through its preservation in a closed system, but to also act as a paleo-piezometer (Alvaro *et al*., 2018) *and* chronometer (Zhong *et al*., 2018).

CONCLUSIONS

The answer to the question which we posed in the Introduction is that inclusions *are* indeed grains of truth, albeit the truth may be occasionally of difficult interpretation. We are also confident that the future study of inclusions, with increasingly subtle and precise analytical tools and theory, will simply confirm what we have already learnt from decades of practice of micropetrology in the investigation of natural rocks using optical microscopes: inclusions in

minerals represent windows through which to peer back into the past history of the host crystal and the rock in which it is contained.

FUNDING

SF was supported by the Alexander von Humboldt Foundation, the German Federal Ministry for Education and Research and the Deutsche Forschungsgemeinschaft (Project FE 1527/2-1 and FE 1527/2-2). RJA was supported by European Research Council (ERC) grant agreements 307322 to Fabrizio Nestola (Padova) and 714936 to Matteo Alvaro (Pavia).

ACKNOWLEDGEMENTS

We are very grateful to the following for providing images and graphics from their own work: XY Gao, Q. Liu, A. Stepanov, S. Ferrando, O. Bartoli, A. Acosta-Vigil, A. Borghini, N. Malaspina, I. Wannhoff, J.A. Axler and T. A. Griffiths. NanoSIMS analyses were performed by L. Remusat at the Muséum National d'Histoire Naturelle, Paris. We thank M. Alvaro, P.J. O'Brien, S. Webb, B. Wunder, M.A. Ziemann, A. Borghini and the students of the TrueDepths project in Pavia for discussions and advice on the topics covered in this paper. Finally the authors are truly grateful to M. Holness for soliciting this manuscript and for her almost infinite patience while it was prepared, as well as for her careful editorial handling, and to B. Cesare and an anonymous reviewer for their insightful reviews which helped us to improve the clarity of the present manuscript.

REFERENCES

Abe, T. & Sunagawa, I. (1995). Hexagonal $CaAl_2Si_2O_8$ in a high-temperature solution: metastable crystallization and transformation of anorthite. *Mineralogical Journal* **17**, 257–281.

Acosta-Vigil, A., Barich, A., Bartoli, O., Garrido, C., Cesare, B., Remusat, L., Poli, S. & Raepsaet, C. 2016. The composition of nanogranitoids in migmatites overlying the Ronda peridotites (Betic Cordillera, S Spain): the anatectic history of a

polymetamorphic basement. *Contributions to Mineralogy and Petrology* 24, 1–31, doi: 10.1007/ s00410-016-1230-3.

Acosta-Vigil, A., Buick, I., Cesare, B., London, D. & Morgan VI, G.B. (2012). The extent of equilibration between melt and residuum during regional anatexis and its implications for differentiation of the continental crust: a study of partially melted metapelitic enclaves. *Journal of Petrology* **53**, 1319–1356.

Acosta-Vigil, A., Buick, I., Hermann, J., Cesare, B., Rubatto, D., London, D. & Morgan VI, G.B. (2010). Mechanisms of crustal anatexis: a geochemical study of partially melted metapelitic enclaves and host dacite, SE Spain. *Journal of Petrology* **51**, 785–821.

Acosta-Vigil, A., Cesare, B., London, D. & Morgan VI, G.B. (2007). Microstructures and composition of melt inclusions in a crustal anatectic environment, represented by metapelitic enclaves within El Hoyazo dacites, SE Spain. *Chemical Geology* **235**, 450–465.

Acosta-Vigil, A., London, D., Morgan, G. B., Cesare, B., Buick, I., Hermann, J. & Bartoli, O. (2017). Primary crustal melt compositions: Insights into the controls, mechanisms and timing of generation from kinetics experiments and melt inclusions. *Lithos* **286–287**, 454–479.

Adams, H. G., Cohen, L. H. & Rosenfeld, J. L. (1975). Solid inclusion piezothermometry I: comparison dilatometry. *American Mineralogist* **60**, 574–583.

Alvaro, M., Angel, R. J., Nimis, P. Milani, S., Harris, J. & Nestola, F. (2017) Orientation relationship between diamond and magnesiochromite inclusions.*Geophysical Research Abstracts* **19**, EGU2017-12200.

Alvaro, M., et al. (2018) Corrections to entrapment pressures of inclusions calculated with isotropic models. *Geology* in prep.

Arlt, T., and Angel, R.J. (2000) Pressure buffering in a diamond anvil cell. *Mineralogical Magazine* **64**, 241-245.

Angel, R. J., Alvaro, M. & Nestola, F. (2018). 40 years of mineral elasticity: a critical review and a new parameterisation of Equations of State for mantle olivines and diamond inclusions. . *Physics and Chemistry of Minerals* **45**, 95-113.

Angel, R. J., Gonzalez-Platas, J. & Alvaro, M. (2014b). EosFit7c and a Fortran module (library) for equation of state calculations. *Zeitschrift für Kristallographie* **229**, 405–419.

Angel, R. J., Mazzucchelli, M. L., Alvaro, M. & Nestola, F. (2017a). EosFit-Pinc: A simple GUI for host-inclusion elastic thermobarometry. *American Mineralogist* **102**, 1957–1960.

Angel, R. J., Mazzucchelli, M. L., Alvaro, M., Nimis, P. & Nestola, F. (2014a). Geobarometry from host-inclusion systems: the role of elastic relaxation. *American Mineralogist* **99**, 2146–2149.

Angel, R. J., Milani, S., Alvaro, M. & Nestola, F. (2015a). OrientXplot – a program to analyse and display relative crystal orientations. *Journal of Applied Crystallography* **48**, 1330–1334.

Angel, R. J., Nimis, P., Mazzucchelli, M. L., Alvaro, M. & Nestola, F. (2015b). How large are departures from lithostatic pressure? Constraints from host-inclusion elasticity. *Journal of Metamorphic Geology* **33**, 801–803.

Ashley, K., Steele-MacInnis, M., Bodnar, R.J., Darling, R.S. (2016) Quartz-in-garnet inclusion barometry under fire: Reducing uncertainty from model estimates. *Geology* **44** (9), 699–702.

Ashley, K., Steele-MacInnis, M., Bodnar, R. J. & Darling, R. S. (2016). Quartz-in-garnet inclusion barometry under fire: Reducing uncertainty from model estimates. *Geology* **44**, 2146–2149.

Audetat, A. & Lowenstern, J.B. (2014). Melt inclusions. In: Holland, H.D., Turekian, K.K. (Eds.) *Treatise on Geochemistry*. Second edition Elsevier, Oxford, 143–173.

Auzanneau, E., Vielzeuf, D. & Schmidt, M.W. (2006). Experimental evidence of decompression melting during exhumation of subducted continental crust. *Contributions to Mineralogy and Petrology* **152**, 125–148.

Axler, J.A. & Ague, J.J. (2015). Oriented multiphase needles in garnet from ultrahigh-temperature granulites, Connecticut, U.S.A. *American Mineralogist* **100**, 2254–2271.

Bakker, R. & Baumgartner, M. (2012). Unexpected phase assemblages in inclusions with ternary H_2O-salt fluids at low temperatures. *Central European Journal of Geosciences* **4**, 225–237.

Barich, A., Acosta-Vigil, A., Garrido, C.J., Cesare, B., Tajčmanová, L. & Bartoli, O. (2014). Microstructures and petrology of melt inclusions in the anatectic sequence of Jubrique (Betic Cordillera, S Spain): implications for crustal anatexis. *Lithos* **206–207**, 303–320.

Bartoli, O. (2018). Reintegrating nanogranitoid inclusion composition to reconstruct the prograde history of melt-depleted rocks. *Geoscience Frontiers*, in press. https://doi.org/10.1016/j.gsf.2018.02.002

Bartoli, O. (2017). Phase equilibria modelling of residual migmatites and granulites: An evaluation of the melt-reintegration approach. *Journal of Metamorphic Geology* **35**, 919–942.

Bartoli, O., Acosta-Vigil, A., Ferrero, S. & Cesare, B. (2016). Granitoid magmas preserved as melt inclusions in high-grade metamorphic rocks. *American Mineralogist* 101, 1543–1559.

Bartoli, O., Cesare, B., Poli, S., Acosta-Vigil, A., Esposito, R., Turina, A., Bodnar, R.J., Angel, R.J. & Hunter, J. (2013a). Nanogranite inclusions in migmatitic garnet: Behavior during piston cylinder re-melting experiments. *Geofluids* **13**, 405–420.

Bartoli, O., Cesare, B., Poli, S., Bodnar, R.J., Acosta-Vigil, A., Frezzotti, M.L. & Meli, S. (2013b). Recovering the composition of melt and the fluid regime at the onset of crustal anatexis and S-type granite formation. *Geology* **41**, 115–118.

Bartoli, O., Cesare, B., Remusat, L., Acosta-Vigil, A. & Poli, S. (2014). The H_2O content of granite embryos. *Earth Planetary Science Letters* **395**, 281–290.

Baxter, E.F. & Scherer, E.E. (2013). Garnet geochronology: timekeeper of tectonometamorphic processes. *Elements* **9**, 433–438.

Berkesi, M., Park, M., Szabó, C., Jung, H. & Kil, Y. (2017). Melt and fluid inclusions in mantle xenoliths beneath the rift shoulder (Adam's diggings) of Rio Grande rift: evidences for metasomatism. European Mineralogical Congress, Rimini.

Bodnar, R.J. (1989). Synthetic fluid inclusions: a novel technique for experimental water-rock interaction studies. In: Water-Rock interaction, Miles (ed.), Balkema-Rotterdam.

Bodnar, R.J. (2003). Reequilibration of fluid inclusions. In: Samson, I., Anderson, A., Marshall, D. (Eds.), Fluid Inclusions: Analysis and Interpretation. *Short Course 32*, Mineralogical Association of Canada, 213–230.

Bodnar, R.J., Lecumberri-Sanchez, P., Moncada, D. & Steele-MacInnis, M. (2014). Fluid inclusions in hydrothermal ore deposits. In: Holland, H.D., Turekian, K.K. (Eds.) *Treatise on Geochemistry*. Second edition Elsevier, Oxford, 119–142.

Borghini, A., Ferrero, S., Wunder, B., O'Brien, P.J., & Ziemann, M.A. (2017). Variscan nanogranitoids in Bohemian Massif orogenic peridotites: evidence for partial melting, metasomatism or both?. International Eclogite Conference, Sweden.

Bose, K. & Ganguly, J. (1995). Quartz-Coesite Transition Revisited - Reversed Experimental-Determination at 500-1200^{o}C and Retrieved Thermochemical Properties. *American Mineralogist* **80**, 231–238.

Boyle, R. (1672). Essay about the origine and virtues of gems. William Godbid, London.

Braga, R. & Massonne, H.J. (2008). Mineralogy of inclusions in zircon from high-pressure crustal rocks from the Ulten Zone, Italian Alps. *Periodico di Mineralogia* **77**, 43–64.

Braga, R., Ferrero, S., Wälle, M. & Remusat, L. (2016). Genesis and evolution of the late Miocene Maghrebian granitoids unraveled through the nanogranites of La Galite archipelago (Tunisia). European Mineralogical Congress, Rimini.

Briggs, R. J. & Ramdas, A. K. (1977). Piezospectroscopy of the Raman spectrum of α-quartz. *Physical Review B* **16**, 3815–3826.

Brown, M. (2007). Crustal melting and melt extraction, ascent and emplacement in orogens: Mechanisms and consequences. *Journal of Geological Society* **164**, 709–730.

Brown, M., (2013). Granite: from genesis to emplacement. Geological Society of American Bulletin, 125, 1079–1113.

Bruno, M., Massaro, F. R., Prencipe, M., Demichelis, R., De La Pierre, M. & Nestola, F. (2014). Ab initio calculations of the main crystal surfaces of forsterite (Mg_2SiO_4): a preliminary study to understand the nature of geochemical processes at the olivine interface. *Journal of Physical Chemistry C* **118**, 2498−2506.

Carlson, W. D., Pattison, D. R. M. & Caddick, M. J. (2015). Beyond the equilibrium paradigm: How consideration of kinetics enhances metamorphic interpretation. *American Mineralogist* **100**, 1659–1667.

Carlson, W. D. & Gordon, C. L. (2004). Effects of matrix grain size on the kinetics of intergranular diffusion. *Journal of Metamorphic Geology* **22**, 733–742.

Carrington, D.P., Harley, S.L. (1995). Partial melting and phase relations in high-grade metapelites: an experimental petrogenetic grid in the KFMASH system. *Contribution to Mineralogy and Petrology* 120, 270–291.

Cesare, B. (2008). Crustal melting: working with enclaves. In: Sawyer, E.W., Brown, M. (Eds.), Working with Migmatites, Short Course 38. Mineralogical Association of Canada, Quebec City, 37–55.

Cesare, B., Acosta-Vigil, A., Bartoli, O. & Ferrero, S. (2015). What can we learn from melt inclusions in migmatites and granulites? *Lithos* **239**, 186–216.

Cesare, B., Acosta-Vigil, A., Ferrero, S. & Bartoli, O. (2011). Melt Inclusions in Migmatites and Granulites paper 2 In: Forster, M.A., Fitz Gerald, J.D. (Eds.) *The Science of Microstructure* — Part II, Electronic edition. Journal of the Virtual Explorer 38 (paper 2).

Cesare, B., Ferrero, S., Salvioli-Mariani, E., Pedron, D. & Cavallo, A. (2009). Nanogranite and glassy inclusions: the anatectic melt in migmatites and granulites. *Geology* **37**, 627–630.

Cesare, B., Rubatto, D. & Gómez-Pugnaire, M.T., (2009b). Do extrusion ages reflect magma generation processes at depth? An example from SE Spain. *Contributions to Mineralogy and Petrology* **157**, 267–279.

Cheskonov, B.V., Lotova, E.V., Pavlyuchenko, V.S., Usova, L.V., Bushmakin, A.F. & Nishanbayev, T.P. (1989). Svyatoslavite $CaAl_2Si_2O_8$: (orthorhombic) – A new mineral. *Zap. Vses. Mineral. Obshch.* **118,** 111–114 (in Russian).

Chopin, C. (1984). Coesite and pure pyrope in high-grade blueschists of the Western Alps: a first record and some consequences. *Contributions to Mineralogy and Petrology* **86**, 107–118.

Clemens, J.D. & Wall, V.J. (1981). Crystallization and origin of some peraluminous (S-type) granitic magmas. *Canadian Mineralogist* **19**, 111–131.

Connolly, J.A.D. (2010). The Mechanics of Metamorphic Fluid Expulsion. Elements **6**, 165–172.

Dabrowski, M., Powell, R. & Podladchikov, Y. (2015). Viscous relaxation of grain-scale pressure variations. *Journal of Metamorphic Geology* **33**, 859–868.

Danyushevsky, L. V., McNeill, A. W. & Sobolev, A. V. (2002). Experimental and petrological studies of melt inclusions in phenocrysts from mantle-derived magmas: An overview of techniques, advantages and complications. *Chemical Geology* **183**, 5–24.

Di Muro, A., Giordano, D., Villemant, B., Montagnac, G., Scaillet, B. & Romano, C. (2006). Influence of composition and thermal history of volcanic glasses on water content as determined by micro-Raman spectrometry. *Applied Geochemistry* **21**, 802–812.

Dingwell, D.B., Romano, C. & Hess, K.-U. (1995). The effect of water on the viscosity of a haplogranitic melt under P–T–X conditions relevant to silicic volcanism. *Contributions to Mineralogy and Petrology* **124**, 19–28.

Eshelby, J. D. (1957). The determination of the elastic field of an ellipsoidal inclusion, and related problems. *Proceedings of the Royal Society of London. Series A. Mathematical and Physical Sciences* **241**, 376–396.

Ferrando, S., Frezzotti, M. L., Dallai, L. & Compagnoni, R. (2005). Multiphase solid inclusions in UHP rocks (Sulu, China): Remnants of supercritical silicate-rich aqueous fluids released during continental subduction. *Chemical Geology* **223**, 68–81.

Ferrando, S., Frezzotti, M.L., Petrelli, M. & Compagnoni, R. (2009). Metasomatism of continental crust during subduction: the UHP whiteschists from the Southern Dora-Maira Massif (Italian Western Alps). *Journal of Metamorphic Geology* **27**, 739–756.

Ferrero, S., Axler, J., Ague, J., Wunder, B. & Ziemann, M.A. (2017). Preserved anatectic melt in ultrahigh-temperature (or high pressure?) felsic granulites, Connecticut, US. European Geosciences Union, Vienna, abstract.

Ferrero, S., Bartoli, O., Cesare, B., Salvioli-Mariani, E., AcostalVigil, A., Cavallo, A., Groppo, C., Battiston, S. (2012). Microstructures of melt inclusions in anatectic metasedimentary rocks. *Journal of Metamorphic Geology* **30**, 303–322.

Ferrero, S., Bodnar, R.J., Cesare, B. & Viti, C. (2011). Re-equilibration of primary fluid inclusions in peritectic garnet from metapelitic enclaves, El Hoyazo, Spain. *Lithos* **124**, 117–131.

Ferrero, S., Braga, R., Berkesi, M., Cesare, B. & Laridhi Ouazaa, N. (2014). Production of metaluminous melt during fluid-present anatexis: an example from the Maghrebian basement, La Galite Archipelago, central Mediterranean. *Journal of Metamorphic Geology* **32**, 209–225.

Ferrero, S., Godard, G., Palmeri, R., Wunder, B. & Cesare, B. (2018a). Partial melting of ultramafic granulites from Dronning Maud Land, Antarctica: constraints from melt inclusions and thermodynamic modeling. *American Mineralogist* **103**, 610–622.

Ferrero, S., O´Brien, P.J., Borghini, A., Wunder, B., Wälle, M., Günter, C., & Ziemann, M.A. (2018b). A treasure chest full of nanogranitoids: an archive to investigate crustal melting in the Bohemian Massif. In: Ferrero, S., Lanari, P., Goncalves, P. & Grosch, E.G. (Eds) *Metamorphic Geology: Microscale to Mountain Belts*. Geological Society, London, Special Publications 478.

Ferrero, S., Wunder, B., Walczak, K., O'Brien, P.J. & Ziemann, M.A. (2015). Preserved near ultrahigh-pressure melt from continental crust subducted to mantle depths. *Geology* **43**, 447–450.

Ferrero, S., Wunder, B., Ziemann, M.A., Wälle, M. & O'Brien, P.J. (2016a). Carbonatitic and granitic melts produced under conditions of primary immiscibility during anatexis in the lower crust. *Earth Planetary Science Letters* **454**, 121–131, doi: 10.1016/j.epsl.2016.08.043.

Ferrero, S., Ziemann, M.A., Angel, R.J., O'Brien, P.J. & Wunder, B. (2016). Kumdykolite, kokchetavite, and cristobalite crystallized in nanogranites from felsic granulites, Orlica□Snieznik Dome (Bohemian Massif): not evidence for ultrahigh□pressure conditions. *Contributions to Mineralogy and Petrology* **171**, 3.

French, B.V., Koeberl, C. (2010) The convincing identification of terrestrial meteorite impact structures: What works, what doesn't, and why. *Earth-Science Reviews* **98**, 123-170.

Frezzotti, M. L. (2001). Silicate-melt inclusions in magmatic rocks: Applications to petrology. *Lithos* **55**, 273–299.

Frezzotti, M.L. & Ferrando, S. (2007). Multiphase solid inclusions in ultrahigh-pressure metamorphic rocks: a petrographic approach. *Periodico di Mineralogia* **76**, 113–125

Frezzotti, M.L. & Ferrando, S. (2015). The chemical behavior of fluids released during deep subduction based on fluid inclusions. *American Mineralogist* 100, 352–377.

Frezzotti, M.L., Tecce, F. & Casagli, A. (2012). Raman spectroscopy for fluid inclusion analysis. *Journal of Geochemical Exploration* **112**, 1–20.

Garcia-Arias, M., Stevens, G., 2017. Phase equilibrium modelling of granite magma petrogenesis: a. An evaluation of the magma compositions produced by crystal entrainment in the source. *Lithos* **277**, 131–153.

Gardien, V., Thompson, A.B., Grujic, D. & Ulmer, P. (1995). Experimental melting of biotite + plagioclase + quartz ± muscovite assemblages and implications for crustal melting. *Journal of Geophysical Research* **100**, 15581–15591.

Gao, X.-Y., Chen, Y.-X. & Zhang, Q.-Q. (2017). Multiphase solid inclusions in ultrahigh-pressure metamorphic rocks: A snapshot of anatectic melts during continental collision. *Journal of Asian Earth Sciences* **145**, 192–204.

Griffiths, T. A., Habler, G. & Abart, R. (2016). Crystallographic orientation relationships in host–inclusion systems: New insights from large EBSD data sets. *American Mineralogist* **101**, 690–705.

Griffiths, T. A., Habler, G., Schantl, P. & Abart, R. (2017). Crystallographic Orientation Relationships (CORs) between rutile inclusions and garnet hosts: towards using COR frequencies as a petrogenetic indicator. *Geophysical Research Abstracts* **19**, EGU2017–7523.

Gualda, G.A.R. & Rivers, M. (2006). Quantitative 3D petrography using X-ray tomography: Application to Bishop Tuff pumice clasts: Journal of Volcanology and Geothermal Research 154, 48–62.

Hacker, B. R. & Gerya, T. (2013). Paradigms, new and old, for ultrahigh-pressure tectonism. *Tectonophysics* **603**, 79–88.

Haifler, J. & Kotková, J. (2016). UHP–UHT peak conditions and near-adiabatic exhumation path of diamond-bearing garnet–clinopyroxene rocks from the Eger Crystalline Complex, North Bohemian Massif. *Lithos* **248-251**, 366–381.

Harlov, D. & Austrheim, H. (2013). Metasomatism and the Chemical Transformation of Rock. Lecture Notes in Earth System Sciences, Springer.

Hermann, J. & Rubatto, D. (2014). Subduction of Continental Crust to Mantle Depth: Geochemistry of Ultrahigh-Pressure Rocks. In: Holland, H.D., Turekian, K.K. (Eds.) *Treatise on Geochemistry*. Second edition Elsevier, Oxford, 309–340

Hermann, J. & Spandler, C. (2008). Sediment melts at sub-arc depths: an experimental study: *Journal of Petrology* **49**, 717–740.

Hermann, J., Spandler, C., Hack, A. & Korsakov, A.V. (2006). Aqueous fluids and hydrous melts in high-pressure and ultra-high pressure rocks: Implications for element transfer in subduction zones. *Lithos* **92**, 399–417.

Hobbs, B. E. & Ord, A. (2016). Does non-hydrostatic stress influence the equilibrium of metamorphic reactions? *Earth-Science Reviews* **163**, 190–233.

Holland, T.J.B. & Powell, R. (2011). An improved and extended internally consistent thermodynamic dataset for phases of petrological interest, involving a new equation of state for solids. *Journal of Metamorphic Geology* **29**, 333–383.

Holness, M.B. & Sawyer, E.W. (2008). On the pseudomorphing of melt–filled pores during the crystallization of migmatites. *Journal of Petrology* **49**, 1343–1363.

Holtz, F., Johannes, W., Tamic, N. & Behrens, H. (2001). Maximum and minimum water contents of granitic melts generated in the crust: a re-evaluation and implications. *Lithos* **56**, 1–14.

Howell, D., Wood, I. G., Dobson, D. P., Jones, A. P., Nasdala, L. & Harris, J. W. (2010). Quantifying strain birefringence halos around inclusions in diamond. *Contributions to Mineralogy and Petrology* **160**, 705–717.

Howell, D., Wood, I.G., Nestola, F., Nimis, P., and Nasdala, L. (2012) Inclusions under remnant pressure in diamond: a multi-technique approach. *European Journal of Mineralogy* **24**, 563-573.

Huang, L. & Kieffer, J. (2004). Amorphous-amorphous transitions in silica glass. I. Reversible transitions and thermomechanical anomalies. *Physical Reviews* **69**, 1–11.

Huddlestone-Holmes, C.R. & Ketcham, R.A. (2005). Getting the inside story: using computed X-ray tomography to study inclusion trails in garnet porphyroblasts. American Mineralogist 90, 1–17.

Huddlestone-Holmes, C.R. and Ketcham, R.A. (2010). An X ray computed tomography study of inclusion trail orientations in multiple porphyroblasts from a single sample. Tectonophysics 480, 305–320.

Hwang, S.-L., Shen, P., Chu, H.-T., Yui, T.-F., Liou, J.-G. & Sobolev, N,V. (2009). Kumdykolite, an orthorhombic polymorph of albite, from the Kokchetav ultrahigh-pressure massif, Kazakhstan. *European Journal of Mineralogy* **21**, 1325–1334.

Hwang, S.-L., Shen, P., Chu, H.T., Yui, T.F., Liou, J.G., Sobolev, N.V., Zhang, R.Y., Shatsky, V.S. & Zayachkovsky, A.A. (2004). Kokchetavite: a new polymorph of $KAlSi_3O_8$ from the Kokchetav UHP terrain. *Contributions to Mineralogy and Petrology* **148**, 380–389.

Izraeli, E., Harris, J. & Navon, O. (1999). Raman barometry of diamond formation. *Earth and Planetary Science Letters* **173**, 351–360.

Jamtveit, B., & Austrheim, H. (2010). Metamorphism: The Role of Fluids. *Elements* **6**, 153–158

Johannes, W. & Holtz, F. (1996). Petrogenesis and experimental petrology of granitic rocks: Berlin, Springer.

Kanzaki, M., Xue, X., Amalberti, J. & Zhang, Q. (2012). Raman and NMR spectroscopic characterization of high-pressure K-cymrite ($KAlSi_3O_8$ H_2O) and its anhydrous form (kokchetavite). *Journal of Mineralogical and Petrological Science* **107**, 114–119.

Van den Kerkhof, A.M., Touret, J.L.R., Mayer, C. & Jansen, J.B.H. 1991. Retrograde methane-dominated fluid inclusions from high-temperature granulites of Rogaland, southwestern Norway. *Geochimica et Cosmochimica Acta* 55, 2533–2544.

Klonowska, I., Janák, M., Majka, J., Petrik, I, Froitzheim, N., Gee, D.G. & Sasinkova, V. (2017). Microdiamond on Areskutan confirms regional UHP metamorphism in the Seve Nappe Complex of the Scandinavian Caledonides. *Journal of metamorphic Geology* **35**, 541–564.

Knoche, R., Dingwell, D. B. & Webb, S. L. (1992). Non-linear temperature dependence of liquid volumes in the system albite-anorthite-diopside. *Contributions to Mineralogy and Petrology* **111**, 61–73.

Kohn, M.J. (2014) "Thermoba-Raman-try": Calibration of spectroscopic barometers and thermometers for mineral inclusions. *Earth and Planetary Science Letters* **388**, 187-196.

Kotková, J., O'Brien, P. J. & Ziemann, M. A. (2011). Diamond and coesite discovered in Saxony-type granulite: Solution to the Variscan garnet peridotite enigma. . *Geology* **39**, 667–670.

Kotková, J., Škoda, R. & Machovič, V. (2014). Kumdykolite from the ultrahigh-pressure granulite of the Bohemian Massif. *American Mineralogist* **99**, 1798–1801.

Kouketsu, Y., Hattori, K., Guillot, S. & Rayner, N. (2016). Eocene to Oligocene retrogression and recrystallization of the Stak eclogite in northwest Himalaya. *Lithos* **240-243**, 155–166.

Kouketsu, Y., Nishiyama, T., Ikeda, T. & Enami, M. (2014). Evaluation of residual pressure in an inclusion–host system using negative frequency shift of quartz Raman spectra. *American Mineralogist* **99**, 433–442.

Krogh, E. J. (1982). Metamorphic evolution of Norwegian country-rock eclogites, as deduced from mineral inclusions and compositional zoning in garnets. *Lithos* **15**, 305–321.

Kueter, N., Soesilo, J., Fedortchouk, Y., Nestola, F., Belluco, L., Troch, J., Wälle, M., Guillong, M., Von Quadt, A. & Driesner, T. (2016). Tracing the depositional history of Kalimantan diamonds by zircon provenance and diamond morphology studies. *Lithos* **265**, 159–176.

Laurie, A. & Stevens, G., 2012. Water-present eclogite melting to produce Earth's early felsic crust. *Chemical Geology* **314–317**, 83–95.

Lecumberri-Sanchez, P., Steele-MacInnis, M. & Bodnar, R.J. (2015). Synthetic fluid inclusions XIX. Experimental determination of the vapor-saturated liquidus of the system H_2O–NaCl–$FeCl_2$. *Geochimica et Cosmochimica Acta* **148**, 34–49.

Li, W.-C., Chen, R.-X., Zheng, Y.F., Tang, H. & Hu, Z. (2016).Two episodes of partial melting in ultrahigh-pressure migmatites from deeply subducted continental crust in the Sulu orogen, China. *GSA Bulletin* **128** (9-10), 1521–1542.

Liu, J., Cheng, N., Yijie, G., Guo, S. & Chen, Y. (2015). Diamond-bearing nano-granitic inclusions in zircons from stromatic metatexite migmatites from the Sulu UHPM belt. International Eclogite Conference, Dominican Republic.

Lofgren, G. (1974). An Experimental Study of Plagioclase Crystal Morphology: Isothermal Crystallization. *American Journal of Science*, 243–273.

Luth, R. W. & Stachel, T. (2014). The buffering capacity of lithospheric mantle: implications for diamond formation. *Contributions to Mineralogy and Petrology* **168**, 1083.

Malaspina, N., Hermann, J., Scambelluri, M. &Compagnoni, R. (2006). Polyphase inclusions in garnet-orthopyroxenite (Dabie Shan, China) as monitors for metasomatism and fluid-related trace element transfer in subduction zone peridotite. *Earth and Planetary Science Letters* **249**, 173–187.

Malaspina, N., Langenhorst, F., Tumiati, S., Campione, M., Frezzotti, M.L., & Poli, S. (2017). The redox budget of crust-derived fluid phases at the slab-mantle interface. *Geochimica et Cosmochimica Acta* **209**, 70–84.

Mancktelow, N. S. (1995). Nonlithostatic pressure during sediment subduction and the development and exhumation of high pressure metamorphic rocks. *Journal of Geophysical Research B* **100**, 571–583.

Marchildon, N. & Brown, M. (2001). Melt segregation in late syn-tectonic anatectic migmatites: An example from the Onawa contact aureole, Maine, USA. *Physics and Chemistry of the Earth, Part A: Solid Earth and Geodesy* **26**, 225–229.

Majka, J., Rosén, Å, Janák, M., Froitzheim, N., Klonowska, I., Manecki, M., Sasinková, V. & Yoshida, K. (2014). Microdiamond discovered in the Seve Nappe (Scandinavian Caledonides) and its exhumation by the "vacuum-cleaner" mechanism. *Geology* **42**, 1107–1110.

Mazzucchelli, M.L., Burnley, P., Angel, R.J., Morganti, S., Domeneghetti, M.C., Nestola, F., and Alvaro, M. (2018a) Elastic geothermobarometry: Corrections for the geometry of the host-inclusion system. *Geology*, **46**, 231-234.

Mazzucchelli, M.L., et al. (2018b) Relaxation in anisotropic inclusion crystals. In prep

Ménez, B., Simionovici, A., Philippot, P., Bohic, S., Gibert, F. Chukalina, M. (2001). X-ray fluorescence micro-tomography of an individual fluid inclusion using a third generation synchrotron light source. In: Nuclear Instruments and Methods in Physics Research Section B: Beam Interactions with Materials and Atoms **181**, 749–754.

Mikhno, A., Musiyachenko, K.A., Shchepetova, O.V., Korsakov, A.V. & Rashchenko, S.V. (2017). CO_2-bearing fluid inclusions associated with diamonds in zircon from the UHP Kokchetav gneisses. *Journal of Raman Spectroscopy*, DOI 10.1002/jrs.5139.

Milani, S., Nestola, F., Alvaro, M., Pasqual, D., Mazzucchelli, M. L., Domeneghetti, M. C. & Geiger, C. (2015). Diamond–garnet geobarometry: The role of garnet compressibility and expansivity. *Lithos* **227**, 140–147.

Milani, S., Nestola, F., Angel, R. J., Nimis, P. & Harris, J. (2016). Crystallographic orientations of olivine inclusions in diamonds. *Lithos* **265**, 312–316.

Morgan, G.B., IV & London, D. (2005). Effect of current density on the electron microprobe analysis of alkali aluminosilicate glasses. *American Mineralogist* **90**, 1131–1138.

Moulas, E., Podladchikov, Y. Y., Aranovich, L. Y. & Kostopoulos, D. (2013). The problem of depth in geology: when pressure does not translate into depth. *Petrology* **21**, 527–538.

Muncill, G. E. & Lasaga, A. C. (1987). Crystal-growth kinetics of plagioclase in igneous systems: one- atmosphere experiments and application of a simplified growth model. *American Mineralogist* **72**, 299–311.

Murri, M., Mazzucchelli, M.L., Campomenosi, N., Korsakov, A.V., Prencipe, M., Mihailova, B.D., Scambelluri, M., Angel, R.J., and Alvaro, M. (2018) Raman elastic geobarometry for anisotropic mineral inclusions. *American Mineralogist*, accepted.

Németh, P, Lehner, S.W., Petaev, M.I. & Buseck, P. (2013). Kumdykolite, a high-temperature feldspar from an enstatite chondrite. *American Mineralogist* **98,** 1070–1073.

Nestola, F., Merli, M., Nimis, P., Parisatto, M., Kopylova, M., De Stefano, A., Longo, M., Ziberna, L. & Manghnani, M. (2012). In situ analysis of garnet inclusion in diamond using single-crystal X-ray diffraction and X-ray micro-tomography. European Journal of Mineralogy 24, 599–606.

Nestola, F., Nimis, P., Angel, R. J., Milani, S., Bruno, M., Prencipe, M. & Harris, J. W. (2014). Olivine with diamond-imposed morphology included in diamond.Syngenesis or protogenesis? *International Geology Review* **56**, 1658–1667.

Nestola, F., Nimis, P., Ziberna, L., Longo, M., Marzoli, A., Harris, J. W., Manghnani, M. H. & Fedortchouk, Y. (2011). First crystal-structure determination of olivine in diamond: composition and implications for provenance in the Earth's mantle. *Earth and Planetary Science Letters* **305**, 249–255.

Neuser, R. D., Schertl, H.-P., Logvinova, A. M. & Sobolev, N. V. (2015). An EBSD study of olivine inclusions in Siberian diamonds: evidence for syngenetic growth? *Russian Geology and Geophysics* **56**, 321–329.

Newcomb, S. (2009). The World in a Crucible: Laboratory Practice and Geological Theory at the Beginning of Geology. Geological Society of America Special Paper, US.

Nimis, P., Alvaro, M., Nestola, F., Angel, R. J., Marquardt, K., Rustioni, G., Harris, J. W. & Marone, F. (2016). First evidence of hydrous silicic fluid films around solid inclusions in gem-quality diamonds. *Lithos* **260**, 384–389.

O'Brien, P.J. (2001). Subduction followed by Collision: Alpine and Himalayan examples. In: Rubie, D.C. & van der Hilst, R. (eds), Processes and Consequences of Deep Subduction, Physics of the Earth and Planetary Interiors **127**, 277–291.

O'Brien, P.J. (1997). Garnet zoning and reaction textures in overprinted eclogites, Bohemian Massif, European Variscides: a record of their thermal history during exhumation. *Lithos* **41**, 119–133.

Palke, A.C., Renfro, N.D. & Berg, R.B. (2017). Melt inclusions in alluvial sapphires from Montana, USA: Formation of sapphires as a restitic component of lower crustal melting? *Lithos* **278–281**, 43–53.

Pamukcu. A.S., Gualda, G.A.R. & Rivers, M.L. (2013). Quantitative 3D petrography using X-ray tomography 4: Assessing glass inclusion textures with propagation phase-contrast tomography. *Geosphere* **9**, 1704–1713.

Papa, S., Pennacchioni, G., Angel, R.J., Faccenda, M. (2018) The fate of garnet during (deep-seated) coseismic frictional heating: The role of thermal shock. *Geology* **46**, 471-474.

Parkinson, C.D. (2000) Coesite inclusions and prograde compositional zonation of garnet in whiteschist of the HP-UHPM Kokchetav massif, Kazakhstan: a record of progressive UHP metamorphism. *Lithos* **52**, 215-233.

Parsons, I., Gerald, J. D. F. & Lee, M. R. (2015). Routine characterization and interpretation of complex alkali feldspar intergrowths. *American Mineralogist* **100**, 1277–1303.

Passchier, C.W. & Trouw, R.A. (2005). Microtectonics. Springer, Berlin.

Patiño-Douce, A.E. & Harris, N. (1998). Experimental constraints on Himalayan anatexis. *Journal of Petrology* **39**, 689–710.

Perraki, M. & Faryad, S.W. (2014). First finding of microdiamond, coesite and other UHP phases in felsic granulites in the Moldanubian Zone: Implications for deep subduction and a revised geodynamic model for Variscan Orogeny in the Bohemian Massif. Lithos 202–203, 157–166.

Perrilllat, J. P., Daniel, I., Lardeaux, J. M. & Cardon, H. (2003). Kinetics of the quartz-coesite transition: application to the exhumation of ultrahigh-pressure rocks. *Journal of Petrology* **44**, 773–788.

Pettke, T. (2006). In-situ laser-ablation-ICP-MS chemical analysis of melt inclusion and prospects for constraining subduction zone magmas. *Mineralogical Association of Canada (MAC) Short Course Series* **36**, 51–80.

Proyer, A., Habler, G., Abart, R., Wirth, R., Krenn, K. & Hoinkes G., (2013). TiO_2 exsolution from garnet by open-system precipitation: evidence from crystallographic and shape preferred orientation of rutile inclusions. *Contributions to Mineralogy and Petrology* **166**, 211.

Putnis, A., Prieto, M. & Fernandez-Diaz, L. (1995). Fluid supersaturation and crystallization in porous media. *Geological Magazine* **132**, 1–13.

Qiong-Xia Xia & Li-Gang Zhou (2017). Different origins of garnet in high pressure to ultrahigh pressure metamorphic rocks. *Journal of Asian Earth Sciences* **145**, 130–148.

Qiu, C., Krüger, Y., Wilke, M., Marti, D., Rička, J. & Frenz, M. (2016). Exploration of the phase diagram of liquid water in the low-temperature metastable region using synthetic fluid inclusions. *Physical Chemistry Chemical Physics* 28227–28241.

Rickers, K., Thomas, R. & Heinrich, W. (2006). The behavior of trace elements during the chemical evolution of the H2O-, B-, and F-rich granite–pegmatite–hydrothermal system at Ehrenfriedersdorf, Germany: a SXRF study of melt and fluid inclusions. *Mineralium Deposita* **41**, 229–245.

Robinson, P., Ross, M., Nord, G. L., Smyth, J. R. & Jaffe, H. W. (1977). Exsolution lamellae in augite and pigeonite: fossil indicators of lattice parameters at high temperature and pressure. *American Mineralogist* **62**, 857–873.

Roedder, E. (1967). Metastable Superheated Ice in Liquid-Water Inclusions under High Negative Pressure. *Science*, 1413–1417.

Roedder, E. (1971). Metastability in Fluid Inclusions. *The Society of Resource Geology*, 327–334.

Roedder, E., (1984). Fluid Inclusions. *Reviews in Mineralogy* **12**. Mineralogical Society of America, Washington, DC.

Rosenfeld, J. L. & Chase, A. B. (1961). Pressure and temperature of crystallization from elastic effects around solid inclusion minerals? *American Journal of Science* **259**, 519–541.

Sawyer, E.W., Cesare, B. & Brown, M. (2011).When the continental crust melts. *Elements* **7**, 229–234.

Scambelluri, M. & Philippot, P. (2001). Deep fluids in subduction zones. *Lithos* **55**, 213-227

Schertl, H. P., Schreyer, W. & Chopin, C. (1991). The Pyrope-Coesite Rocks and Their Country Rocks at Parigi, Dora Maira Massif, Western Alps - Detailed Petrography, Mineral Chemistry and Pt-Path. *Contributions to Mineralogy and Petrology* **108**, 1–21.

Schairer, J.F. & Bowen, N.L. (1956). The system Na_2O-Al_2O_3-SiO_2. American Journal of Science, **254**, 129-196.

Schmalholz, S. M. & Podladchikov, Y. (2013). Tectonic overpressure in weak crustal-scale shear zones and implications for the exhumation of high-pressure rocks. *Geophysical Research Letters* **40**, 1984–1988.

Schmalholz, S. M. & Podladchikov, Y. (2014). Metamorphism under stress: The problem of relating minerals to depth. *Geology* **42**, 733–734.

Schmidt, C. & Ziemann, M. A. (2000). In-situ Raman spectroscopy of quartz: A pressure sensor for hydrothermal diamond-anvil cell experiments at elevated temperatures. *American Mineralogist* **85**, 1725–1734.

Sirbescu, M. C., Zielinski, N. J., Wilke, M. & Schmidt, C. (2016). What does it take to make a pegmatite ? Direct observations of crystal nucleation and growth. 2015–2017.

Sirbescu, M. L. C., Schmidt, C., Veksler, I. V., Whittington, A. G. & Wilke, M. (2017). Experimental crystallization of undercooled felsic liquids: Generation of pegmatitic texture. *Journal of Petrology* **58**, 539–568.

Słupski, P., Ferrero, S. & Walczak, K. (2018). Former melt inclusions in garnets from granulites of the Góry Sowie Block, NE Bohemian Massif. *Geophysical Research Abstracts*, 20, EGU2018-15214.

Sobolev, N. V. (1977). Deep-seated inclusions in kimberlites and the problem of the composition of the upper mantle. Washington DC: American Geophysical Union.

Sorby, H.C. (1858). On the microscopical structure of crystals, indicating origin of minerals and rocks. *Quarterly Journal of the Geological Society of London* **14**, 453–500.

Spear, F. S., Pattison, D. R. M., & Cheney, J. T. (2016). The metamorphosis of metamorphic petrology. *Geological Society of America Special Papers* **523**, 31–74.

Spear, F. S., Thomas, J. B. & Hallet, B. W. (2014). Overstepping the garnet isograd: a comparison of QuiG barometry and thermodynamic modeling. *Contributions to Mineralogy and Petrology* **168**, 1059.

Spear, F.S., 1993. Metamorphic Phase Equilibria and Pressure-Temperature-Time Paths. Mineralogical Society of America, Washington, DC.

Stachel, T. & Luth, R. W. (2015). Diamond formation — where, when and how? *Lithos* **220–223**, 200–220.

Sterner, S.M. & Bodnar, R.J, 1984. Synthetic fluid inclusions in natural quartz. I. Compositional types synthesized and applications to experimental geochemistry. *Geochimica et Cosmochimica Acta* **48**, 2659–2668.

Steele-MacInnis, M., Lecumberri-Sanchez, P., Bodnar, R.J. (2015). Synthetic fluid inclusions XX. Critical PTx properties of H_2O–$FeCl_2$ fluids. *Geochimica et Cosmochimica Acta* **148**, 50–61.

Stevens, G., Clemens, J.D. & Droop, G.T.R. (1997). Melt production during granulite-facies anatexis: experimental data from "primitive" metasedimentary protoliths. *Contributions to Mineralogy and Petrology* **128**, 352–370.

Stöckhert, B., Trepmann, C.A. & Massonne H.J. (2009). Decrepitated UHP fluid inclusions: about diverse phase assemblages and extreme decompression rates (Erzgebirge, Germany). *Journal of Metamorphic Geology* **27**, 673–684.

Student, J.J. & Bodnar, R.J. (1999). Synthetic Fluid Inclusions XIV: Coexisting Silicate Melt and Aqueous Fluid Inclusions in the Haplogranite–H_2O–NaCl–KCl System. *Journal of Petrology* **40**, 1509–1525.

Tacchetto, T., Bartoli, O., Cesare, B., Berkesi, M., Aradi, L.E., Dumond, G. & Szabó, C. (2018) Multiphase inclusions in peritectic garnet from granulites of the Athabasca granulite terrane (Canada): Evidence of carbon recycling during Neoarchean crustal melting. Chemical Geology, in press.

Tait, S., 1992. Selective preservation of melt inclusions in igneous phenocrysts. *American Mineralogist* **77**, 146–155.Tajčmanová, L., Podladchikov, Y., Powell, R., Moulas, E., Vrijmoed, J. & Connolly, J. A. D. (2014). Grain-scale pressure variations and chemical equilibrium in high-grade metamorphic rocks. *Journal of Metamorphic Geology* **32**, 195–207.

Tajčmanová, L., Vrijmoed, J. & Moulas, E. (2015). Grain-scale pressure variations in metamorphic rocks: implications for the interpretation of petrographic observations. *Lithos* **216-217**, 338–351.

Tamic, N., Behrens, H. & Holtz, F. (2001). The solubility of H_2O and CO_2 in rhyolitic melts in equilibrium with a mixed CO_2–H_2O fluid phase. *Chemical Geology* **174**, 333–347.

Taylor, L. A., Anand, M., Promprated, P., Floss, C. & Sobolev, N. V. (2003). The significance of mineral inclusions in large diamonds from Yakutia, Russia. *American Mineralogist* **88**, 912–920.

Thomas, J.B., and Spear, F.S. (2018) Experimental study of quartz inclusions in garnet at pressures up to 3.0 GPa: evaluating validity of the quartz-in-garnet inclusion elastic thermobarometer. *Contributions to Mineralogy and Petrology* **173**, 42.

Thomas, R., Webster, J. D. & Heinrich, W. (2000). Melt inclusions in pegmatite quartz: complete miscibility between silicate melts and hydrous fluids at low pressure. *Contributions to Mineralogy and Petrology* **139**, 394–401.

Thompson, A. B., Tracy, R. J., Lyttle, P. & Thompson Jr., J. B. (1977). Prograde reactions histories deduced from compositional zonation and mineral inclusions in garnet from the Gassetts schists, Vermont. *American Journal of Science* **277**, 1152–1167.

Torquato, S. (2002). *Random Heterogeneous Materials: Microstructure and Macroscopic Properties*. New York: Springer-Verlag.

Touret, J.L.R. (1981). Fluid inclusions in high grade metamorphic rocks. In: Hollister, L.S., Crawford, M.L. (Eds.), Short Course in Fluid Inclusions: Applications to Petrology. Mineralogical Association of Canada, Calgary, 182–208.

Touret, J.L.R. (2009). Mantle to lower-crust fluid/melt transfer through granulite metamorphism. *Russian Geology and Geophysics* **50**, 1052–1062.

Tracy, R. J., Robinson, P. & Thompson, A. B. (1976). Garnet composition and zoning in the determination of temperature and pressure of metamorphism, central Massachusetts. *American Mineralogist* **61**, 762–775.

Vernon, R.H. (2011). Microstructures of melt-bearing regional metamorphic rocks. In: Van Reenen, D.D., Kramers, J.D., McCourt, S. & Perchuk, L.L. (eds), Origin and Evolution of Precambrian High-Grade Gneiss Terranes, with Special Emphasis on the Limpopo Complex of Southern Africa. Geological Society of America Memoir 207, 1–11.Zhang, Y. (1998) Mechanical and phase equilibria in inclusion–host systems. *Earth and Planetary Science Letters* **157**, 209-222.

van der Molen, I. & van Roermund, H. L. M. (1986). The pressure path of solid inclusions in minerals: the retention of coesite inclusions during uplift. *Lithos* **19**, 317–324.

Vielzeuf, D. & Clemens, J.D. (1992). Fluid-absent melting of phlogopite + quartz: experiments and models. *American Mineralogist* **77**, 1206–1222.

Vielzeuf, D. & Montel, J.M. (1994). Partial melting of Al-metagraywackes. Part 1: Fluid-absent experiments and phase relationships. *Contributions to Mineralogy and Petrology* **117**, 375–93.

Viete, D.R., Hacker, B.R., Allen, M.B., Seward, G.E.G., Tobin, M.J., Kelley, C.S., Cinque, G., and Duckworth, A.R. (2018) Metamorphic records of multiple seismic cycles during subduction. *Science Advances* **4**, eaaq0234.

Vityk, M.O., Bodnar, R.J. & Doukhan, J.C. (2000). Synthetic fluid inclusions: XV. TEM investigationof plastic flow associated with re-equilibration of synthetic fluid inclusions in natural quartz. *Contributions to Mineralogy and Petrology* **139**, 285–297.

Vrijmoed, J., Podladchikov, Y., Anderson, T. B. & Hartz, E. H. (2009). An alternative model for ultra-high pressure in the Svartberget Fe-Ti garnet-peridotite, Western Gneiss Region, Norway. *European Journal of Mineralogy* **21**, 1119–1133.

Wang, L., Zhang, Y. & Essene, E. J. (1996). Diffusion of the hydrous component in pyrope. *American Mineralogist* **81**, 706–718.

White, R., Stevens, G. & Johnson, T. E. (2011). Is the crucible reproducible? Reconciling melting experiments with thermodynamic calculations. *Elements* **7**, 241–246.

Whitney, D. L. (1991). Calcium depletion halos and Fe-Mn-Mg zoning around faceted plagioclase inclusions in garnet from a high-grade pelitic gneiss. *American Mineralogist* **76**, 493–500.

Whitney, D. L., Cooke, M. L. & Du Frane, S. A. (2000). Modeling of radial microcracks at corners of inclusions in garnet using fracture mechanics. *Journal of Geophysical Research B* **105**, 2843—2853.

Whitney, D. L. & Evans, B. W. (2010). Abbreviations for names of rock–forming minerals. *American Mineralogist* **95**, 185–187.

Williame, C. & Brown, W. L. (1974). A coherent elastic model for the determination of the orientation of exsolution boundaries: application to feldspars. *Acta Crystallographica A* **30**, 316–331.

Wilke, F.D.H., O'Brien, P.J., Schmidt, A. & Ziemann, M.A. (2015). Subduction, peak and multistage exhumation metamorphism: traces from one coesite-bearing eclogite, Tso Morari, western Himalaya. *Lithos* **231**, 77–91.

Wirth, R., (2009). Focused Ion Beam (FIB) combined with SEM and TEM: Advanced analytical tools for studies of chemical composition, microstructure and crystal structure in geomaterials on a nanometre scale. *Chemical Geology* **261**, 217–229.

Wolfe, O.M., and Spear, F.S. (2018) Determining the amount of overstepping required to nucleate garnet during Barrovian regional metamorphism, Connecticut Valley Synclinorium. *Journal of Metamorphic Geology* **36**, 79-94.

Xia, Q. X. & Zhou, L. G. (2016). Different origins of garnet in high pressure to ultrahigh pressure metamorphic rocks. *Journal of Asian Earth Sciences*. Elsevier **145**, 130–148.

Yakymchuk, C., & Brown, M. (2014). Consequences of open-system melting in tectonics. *Journal of the Geological Society* **171**, 21–40.

Yardley, B. W. D., Mackenzie, W. S. & Guilford, C. (1991). Atlas of metamorphic rocks and their textures. *Terra Nova* **3**, 217–218.

Yardley, B.W.D. (2009). The role of water in the evolution of the continental crust. *Journal of the Geological Society* **166**, 585–600.

Yoshida, K., Hirajima, T., Miyake, A., Tsuchiyama, A., Ohi, S., Nakano, T. & Uesugi, K. (2016). Combined FIB microsampling and X-ray microtomography: a powerful tool for the study of tiny fluid inclusions. *European Journal of Mineralogy* **28**, 245–256.

Zhang, Z. & Duan, Z. (2005). Prediction of the PVT properties of water over wide range of temperatures and pressures from molecular dynamics simulation. *Physics of the Earth and Planetary Interiors* **149**, 335–354.
Zhao, J., Angel, R. J. & Ross, N. L. (2011). The structural variation of rhombohedral $LaAlO_3$ perovskite under non-hydrostatic stress fields in a diamond–anvil cell. *Journal of Physics C: Condensed Matter* **23**, 175901.
Zhong, X., Moulas, E., and Tajčmanová, L. (2018) Tiny timekeepers witnessing high-rate exhumation processes. *Science Reports* **8**, 2234.

FIGURE CAPTIONS

Figure 1. Isomekes for garnet and diamond (grey lines) calculated with EosFit7c (Angel *et al*., 2014a). The blue line is the graphite-diamond equilibrium phase boundary. All entrapment isomekes from the diamond stability field have $P > 0$ at room temperature. The yellow areas are where the inclusion pressure is higher than the external pressure; $P_{inc} > P_{ext}$. (a) Any garnet inclusion trapped inside a diamond while the diamond grew in its stability field should exhibit a positive remnant pressure P_{inc} when the diamond host is at room conditions. (b) Conversely, a diamond trapped inside a garnet that grew in the diamond stability field should exhibit a negative (or zero) remnant pressure P_{inc} when the garnet host is at room conditions. (c) Positive remnant pressures in diamond inclusions in garnet indicate that elastic resetting has occurred at high T in the graphite stability field, creating a reset isomeke that passes through room T at negative pressures.

Figure 2: (a) Evolution of the inclusion Pthermo and Pinc in a coesite inclusion in garnet, trapped at ~3.7 GPa and 800 C, if no transition from coesite to quartz occurs. The unusual increase in inclusion pressures at lower temperatures is due to the anomalously-low thermal expansion coefficient of coesite, that is also responsible for the isomekes with garnet (grey lines) having strongly negative slopes. (b) Schematic of possible inclusion pressure paths (blue arrows) for different behaviour of the inclusion. If the kinetics of the coesite to quartz

transition are fast enough, the volume expansion of the host garnet is accommodated by the transformation of coesite to quartz, leading to the inclusion pressure being buffered to the transition boundary (black line). If the kinetics slow, then the inclusion pressure drops below the boundary pressure (Perrillat *et al*., 2003), but total pressure loss only occurs if silica is removed from the inclusion (lowest blue arrow).

Figure 3. Occurrence of different Al_2SiO_5 polymorphs in garnet porphyroblasts from the Jubrique unit, Betic Cordillera, Spain. The figures have been provided by A. Acosta-Vigil and modified after Barich *et al*. (2014). (a) Sillimanite mineral inclusions (red arrows) occur at the garnet rim, while at the garnet core (b) kyanite often occurs as trapped mineral inclusion in nanogranitoids (black arrows). Here and everywhere else in this work we use mineral abbreviations from Whitney & Evans (2010).

Figure 4: Nanogranitoids, or former melt inclusions of anatectic origin. (a) Optical appearance between parallel (left) and crossed polars (right) of nanogranitoids in ultramafic granulites from Dronning Maud Land, Antarctica (Ferrero *et al*., 2018); (b) Back Scattered Electron (BSE) image of an inclusion cluster in a high-pressure garnet clinopyroxenite from the Granultigebirge, Bohemian Massif (image courtesy of A. Borghini). All the inclusions contain phases consistent with melt crystallization and can be re-homogenized to a hydrous glass (Borghini *et al*., 2017); (c) BSE image of inclusion in a medium pressure khondalite from the Kerala Khondalite Belt, Southern India (S. Ferrero, PhD thesis); (d) BSE image of nanogranitoids in a low-to-medium pressure migmatite from the Bayerische Wald (Stückstein), Moldanubian Zone, Bohemian Massif (image courtesy of I. Wannhoff); (e) and (f) BSE images of inclusions interpreted as former MI in zircon and titanite from UHP migmatites of the Sulu orogen (images courtesy of R-X. Chen; see also Li *et al*., 2016).

Figure 5: Tubular and needle-shaped nanogranitoids. (a) Tubular polycrystalline inclusions (black arrows and close-up in the lower left corner) interpreted to be former melt inclusions in a Gore Mountains garnet megacryst (image courtesy of R. Darling, see also Darling *et al*., 1997); (b) BSE image of a needle-shaped nanogranitoid in garnet from a granulite of the Acadian orogeny, northeastern Connecticut (figure modified after Axler & Ague, 2015). In both (a) and (b) most of the inclusions are oriented parallel to exsolved rutile needles in the host garnet.

Figure 6: Melt re-integration procedure applied to partially melted granulitic enclave from El Hoyazo, Neogene Volcanic Province (figures provided by O. Bartoli and modified after Bartoli (2017)). (a) The initial protolith has been back-calculated using both the composition of anatectic MI and of the glass still preserved in the enclave's matrix; the calculated protolith shows a melt productivity of ~50 wt% at 850°C, consistent with petrographic constraints (see discussion in Bartoli *et al.*, 2017).

Figure 7: Nanocarbonatites. (a) BSE image of primary carbonate melt droplets in medium pressure migmatite from the Oberpfalz, Moldanubian Zone, Bohemian Massif (Ferrero *et al*., 2016). Wm= white mica. (b) Most of the inclusion consists of calcite identified via Raman spectroscopy, along with white mica and chlorite (c). Images and spectra are modified after Ferrero *et al*. (2016).

Figure 8: Polycrystalline inclusions interpreted as former melt droplets in *HP/UHP* rocks; BSE images. (a) Nanogranitoids from the Polish Sudetes, Bohemian Massif (modified after Ferrero *et al*., 2016). *Kml*= kumdykolite; *Kok*= kokchetavite; (b) MSI from the Kokchetav Massif, Kazakhstan (image courtesy of A.Stepanov, modified after Stepanov *et al*., 2016); (c) and (d) MSI from Shuanghe *UHP* eclogites, Dabie-Sulu orogen. Image (c) was provided by

Q.Liu and modified after Liu *et al*., 2013, while (d) is from Gao *et al*. 2013. (e) Fluid inclusion in eclogite-facies Dora Maira whiteschist, modified after Ferrando *et al.* (2009); (f) Multiphase solid inclusion in eclogite-facies Dora Maira whiteschist, modified after Frezzotti & Ferrando (2007).

Figure 9: Residual glass in near-*UHP* nanogranitoids from the Polish Sudetes. (a) Nanogranitoid containing (b) residual glass, as visible from the Raman map of the spectral region 3200-3600 cm^{-1} characteristic of H_2O hosted in glass (modified after Ferrero *et al*., 2016); (c) Raman spectrum of residual glass in near *UHP* nanogranitoid (modified after Ferrero *et al*., 2015). The main peaks of garnet are indicated, along with peaks characteristic of other mineral phases crystallized in nanogranitoids (stars). A hydrous standard glass of granitic composition is reported for comparison (Morgan & London, 2005).

Figure 10: Metastable polymorphs crystallized in nanogranitoids from different *HP* rocks of the Bohemian Massif. (a) BSE images of inclusion in the Orlica-Śnieżnik granulites, modified after Ferrero *et al*. (2016); (b) inclusion in garnet clinopyroxenite from the Granulitgebirge (image courtesy of A. Borghini); (c) PT path followed by nanogranitoids in Orlica-Śnieżnik felsic granulites (modified after Ferrero *et al*., 2016) during cooling. Gray dot: minimum conditions for entrapment ~875°C and ~2.7 GPa (Ferrero *et al*., 2015), for reactions and solidus curves see Ferrero *et al*. (2016). The nanogranitoid path (thick line) is calculated assuming no crystallization even after the path crosses the wet solidus, when the melt enters in an undercooled state. When crystallization ultimately starts (white circle) well below the wet solidus, the P_{inc} drops significantly (dashed line). The T at which crystallization starts is only assumed, as it cannot be easily calculated given our present state of knowledge.

Figure 11: Characteristic Raman spectra of (a) kumdykolite and (b) kokchetavite in a low P nanogranitoid from the La Galite Archipelago (Ferrero, unpublished; BSE image modified after Ferrero et al., 2014).

Figure 12. Qualitative diagram illustrating the evolution of the internal pressure for melt inclusions in garnet with respect to the entrapment isomeke. The pressure in an inclusion (blue line) that is softer than its host, as for MI in garnet, always remains between the external pressure (red line) and the pressure of the entrapment isomeke at the same T. When the rock pressure is below the entrapment isomeke, the inclusion is over-pressured. When the external pressure crosses the entranpment isomeke, the pressure in the inclusion is equal to the external pressure. When the external pressure lies above the entrapment isomeke, the inclusion is at a lower pressure.

Figure 13: Principles of MI pressures illustrated with isomekes (thin lines) for MI in garnets with compositions from Ferrero *et al.* (2016). Key isomekes highlighted with green lines, rock *P-T* path with solid red lines (a) Entrapment at low *P* allows the rock path to take the inclusion to a condition of under-pressure by isobaric cooling after exhumation to shallow crustal levels, and thus promote the crystallisation of low-density 'metastable' polymorphs as the thermodynamically-stable phase in the inclusion. (b) Entrapment at *HP* conditions (example path taken from Fig. 10c) does not allow the rock path cross the entrapment isomeke, nor to cross an isomeke representing elastic resetting at lower pressures. (c) Reheating of the rock, for example during underplating, followed by quasi-isobaric cooling, can lead to under-pressure in the inclusion and the crystallisation of low-density phases.

Figure 14: Preserved water in inclusions from *HP/UHP* rocks. (a) FTIR-FPA map of MSI in a garnet orthopyroxenite from Dabie Shan (image modified after Malaspina *et al*., 2017). The

map shows the intensity of the H_2O band at 1630cm^{-1}, indicated in the spectrum. For more details on the map, see Malaspina *et al*. (2017); (b) BSE image of re-homogenized nanogranitoid in garnet (modified after Ferrero *et al*., 2015) and a plot of measured H_2O contents by Raman and NanoSIMS. The irregular shape of the nanogranitoid is not the result of any interaction with the host, since the chemical composition of the inclusion does not show any evidence of contamination from the host garnet.

Figure 15: Equal angle stereographic projection of the orientation distribution function (ODF) of the c-directions of 250 rutile inclusions in two grains of a pegmatitic garnet, relative to the garnet unit-cell axes (Griffiths *et al.,* 2016). The symmetry of the ODF reflects the symmetry of the garnet host crystal. The rutile inclusions clearly exhibit three distinct types of COR with respect to the garnet. One group of c-directions occurs in a small circle surrounding a high-symmetry direction in garnet (white circles). The second group (black circles) is a dispersional COR concentrated narrowly around a different high symmetry garnet direction. Surrounding this group a more diffuse concentration of c-directions is found (grey circles). For full details of the analysis see Griffiths *et al*. (2016).

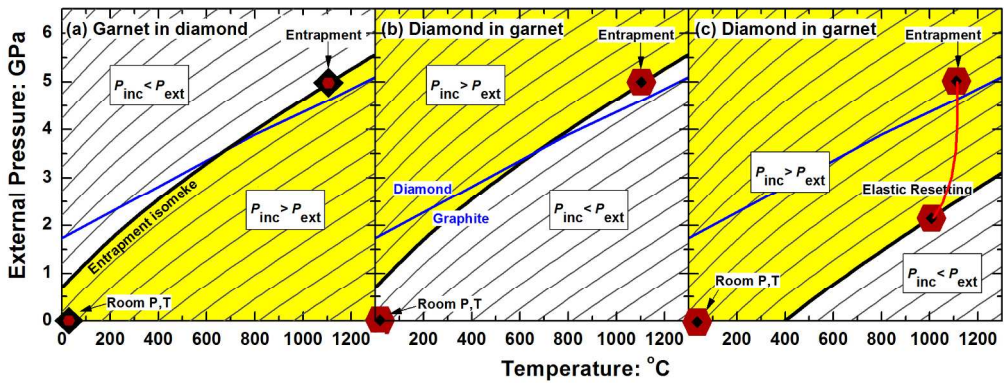

Figure 1: Isomekes for garnet and diamond (grey lines) calculated with EosFit7c (Angel et al. 2014a). The blue line is the graphite-diamond equilibrium phase boundary. All entrapment isomekes from the diamond stability field have P > 0 at room temperature. The yellow areas are where the inclusion pressure is higher than the external pressure; Pinc > Pext. (a) Any garnet inclusion trapped inside a diamond while the diamond grew in its stability field should exhibit a positive remnant pressure Pinc when the diamond host is at room conditions; (b) conversely, a diamond trapped inside a garnet that grew in the diamond stability field should exhibit a negative (or zero) remnant pressure Pinc when the garnet host is at room conditions. (c) Positive remnant pressures in diamond inclusions in garnet indicate that elastic resetting has occurred at high T in the graphite stability field, creating a reset isomeke that passes through room T at negative pressures.

199x75mm (300 x 300 DPI)

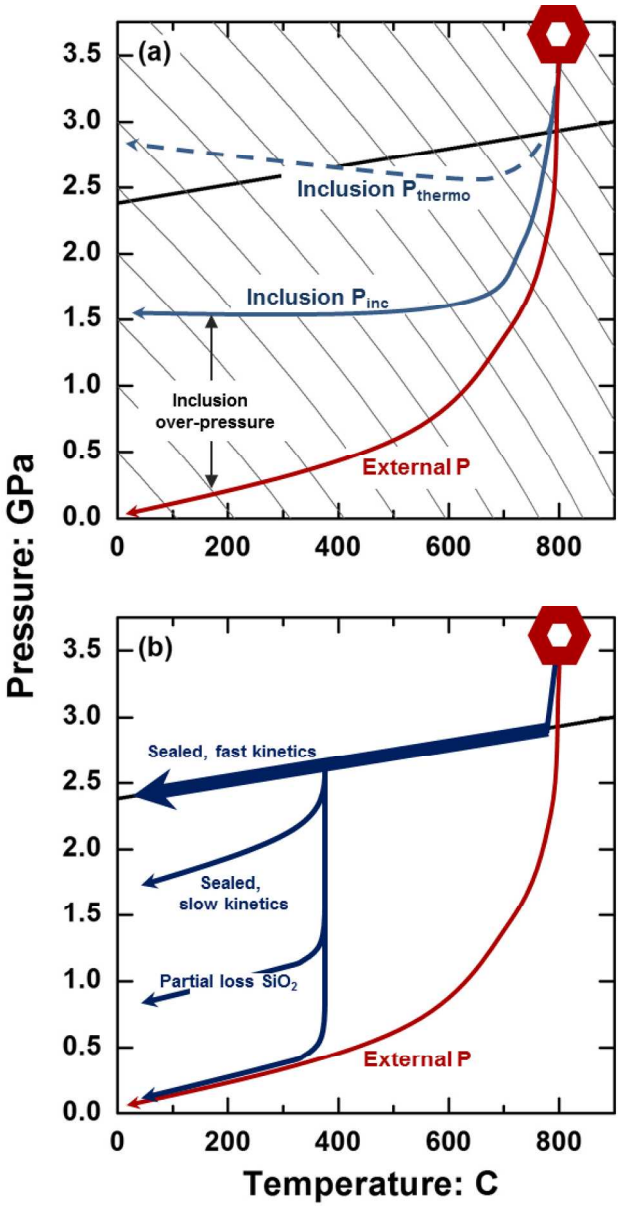

Figure 2: (a) Evolution of the inclusion Pthermo and Pinc in a coesite inclusion in garnet, trapped at ~3.7 GPa and 800C, if no transition from coesite to quartz occurs. The unusual increase in inclusion pressures at lower temperatures is due to the anomalously-low thermal expansion coefficient of coesite, that is also responsible for the isomekes with garnet (grey lines) having strongly negative slopes; (b) schematic of possible inclusion pressure paths (blue arrows) for different behaviour of the inclusion. If the kinetics of the coesite to quartz transition are fast enough, the volume expansion of the host garnet is accommodated by the tramsformation of coesite to quartz, leading to the inclusion pressure being buffered to the transition boundary (black line). If the kinetics slow, then the inclusion pressure drops below the boundary pressure (Perrillat et al. 2003), but total pressure loss only occurs if silica is removed from the inclusion (lowest blue arrow).

100x189mm (300 x 300 DPI)

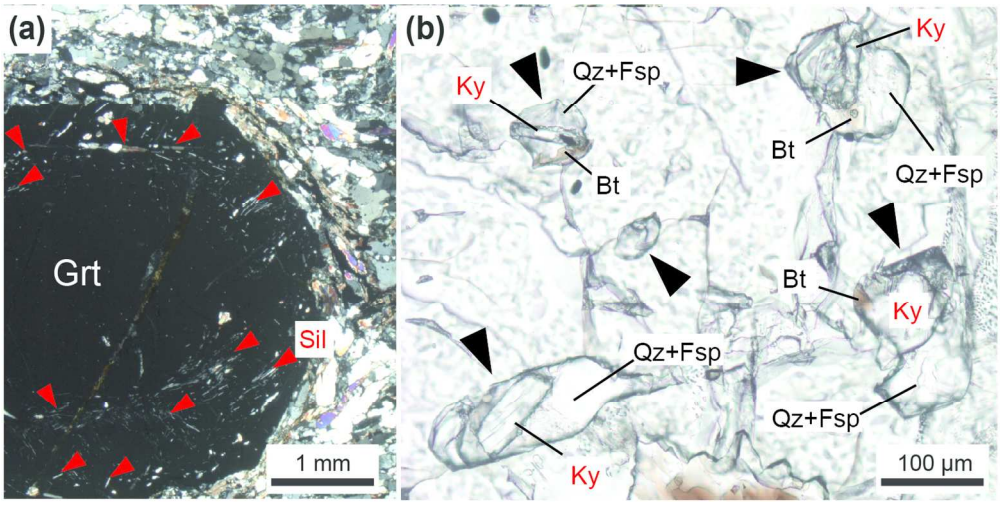

Figure 3. Occurrence of different Al2SiO5 polymorphs in garnet porphyroblasts from Jubrique unit, Betic Cordillera, Spain. The figures have been provided by A. Acosta-Vigil and modified after Barich et al. 2014. (a) Sillimanite mineral inclusions (red arrows) occur at the garnet rim, while at the garnet core (b) kyanite often occurs as trapped mineral inclusion in nanogranitoids (black arrows). Here and everywhere else in the paper we used mineral abbreviations from Whitney & Evans (2010).

141x70mm (300 x 300 DPI)

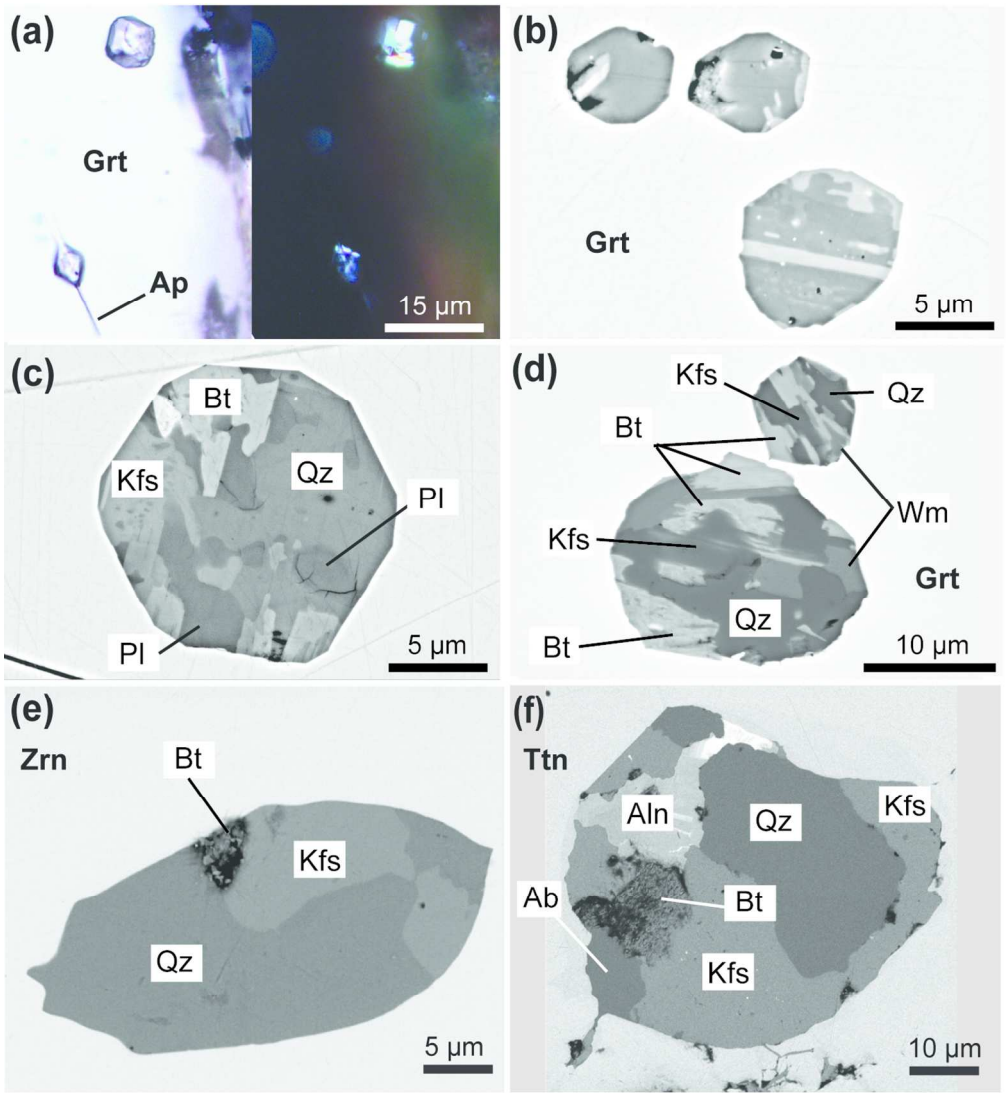

Figure 4. Nanogranitoids, or former melt inclusions of anatectic origin. (a) optical appearance between parallel (left) and crossed polars (right) of nanogranitoids in ultramafic granulites from the Dronning Maud Land, Antarctica (Ferrero et al., 2018); (b) Back Scattered Electrons (BSE) image of an inclusion cluster in high-pressure garnet clinopyroxenites of the Granultigebirge, Bohemian Massif (image courtesy of A. Borghini). All the inclusions contain phases consistent with melt crystallization and can be re-homogenized to a hydrous glass (Borghini et al. 2017); (c) BSE picture of inclusion in medium pressure khondalites of the Kerala Khondalite Belt, Southern India (S. Ferrero, PhD thesis); (d) BSE image of nanogranitoids in low-to-medium pressure migmatites from the Bayerische Wald (Stückstein), Moldanubian Zone, Bohemian Massif (image courtesy of I. Wannhoff); (c) and (d) BSE images of inclusions interpreted as former MI in zircon and titanite from UHP migmatites of the Sulu orogen (images courtesy of R-X. Chen, see also Li et al. 2016).

120x130mm (300 x 300 DPI)

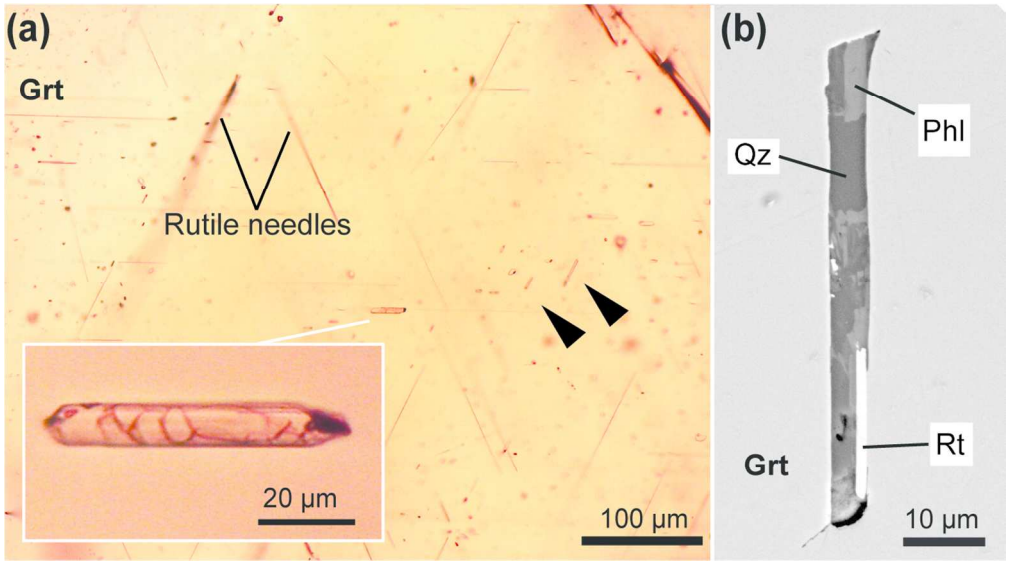

Figure 5: Tubular and needle-shaped nanogranitoids. (a) tubular polycrystalline inclusions (black arrows and close-up in the lower left corner) interpreted to be former melt inclusions in Gore Mountains garnet megacrysts (image courtesy of R. Darling, see also Darlinget al. 1997); (b) BSE image of a needle-shaped nanogranitoid in garnet from granulites of the Acadian orogeny, northeastern Connecticut (figure modified after Axler & Ague, 2015). In both (a) and (b) most of the inclusions are oriented parallel to exsolved rutile needles in the host garnet.

119x66mm (300 x 300 DPI)

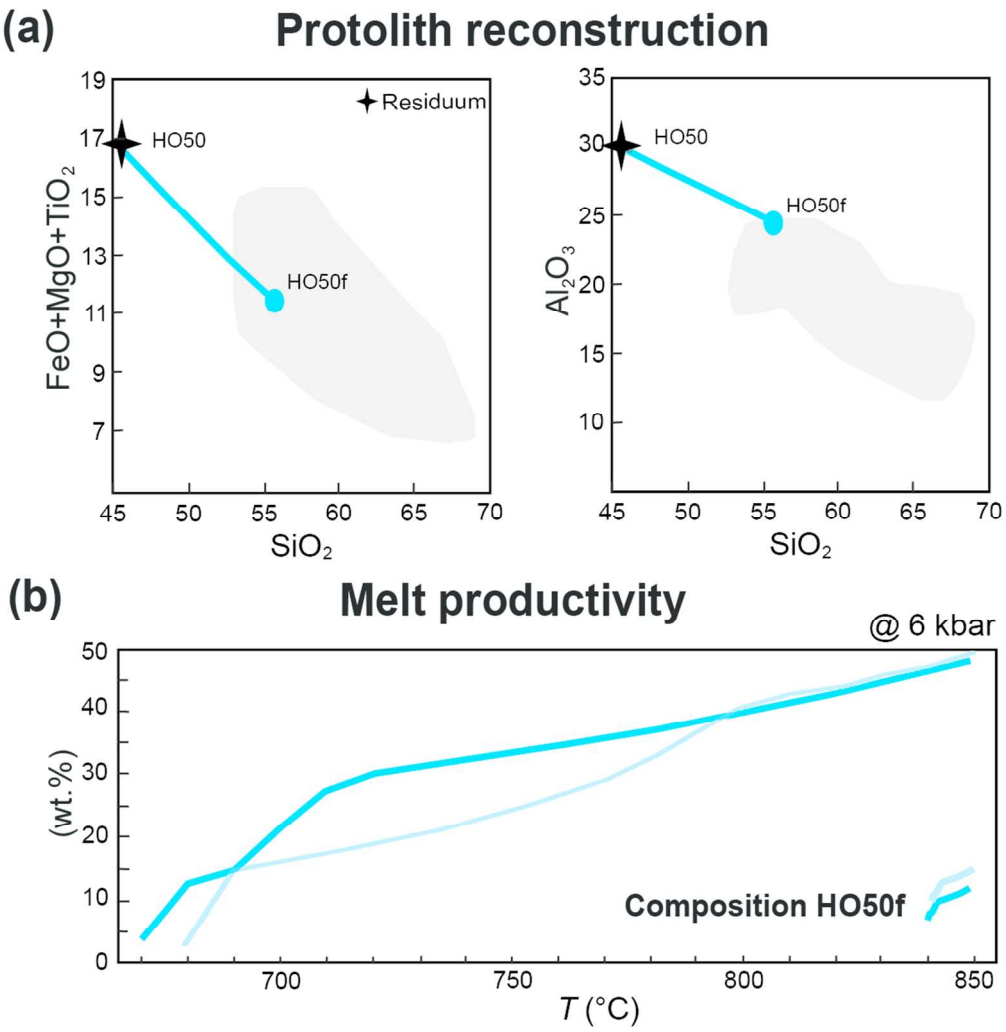

Figure 6. Melt re-integration procedure applied to partially melted granulitic enclaves of El Hoyazo, Neogene Volcanic Province (figures provided by O. Bartoli and modified after Bartoli, 2017). (a) The initial protolith has been back-calculated using both the composition of anatectic MI and of the glass still preserved in the enclaves matrix; the calculated protolith shows a melt productivity of ~50 wt% at 850°C, consistent petrographic constraints (see discussion in Bartoli et la., 2017).

101x104mm (300 x 300 DPI)

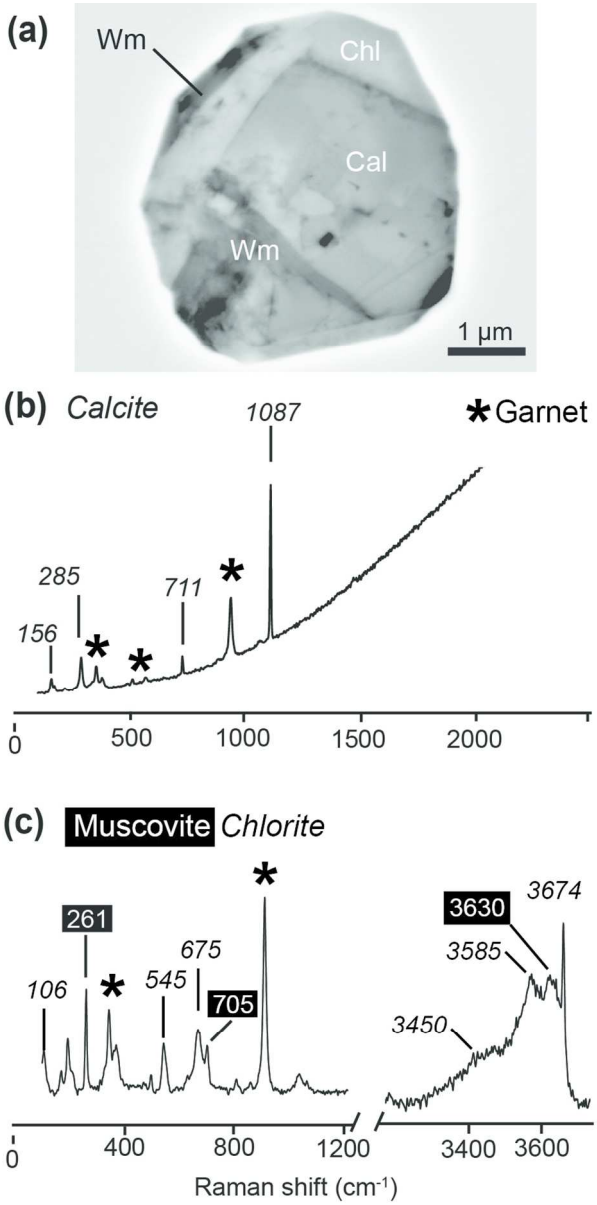

Figure 7. Nanocarbonatites. (a) BSE image of primary carbonate melt droplets in medium pressure migmatites form the Oberpfalz, Moldanubian Zone, Bohemian Massif (Ferrero et al. 2016). Wm= white mica. (b) Most of the inclusion consists of calcite identified via Raman spectroscopy, along with white mica and chlorite (c). Images and spectra are modified after Ferrero et al. (2016).

77x152mm (300 x 300 DPI)

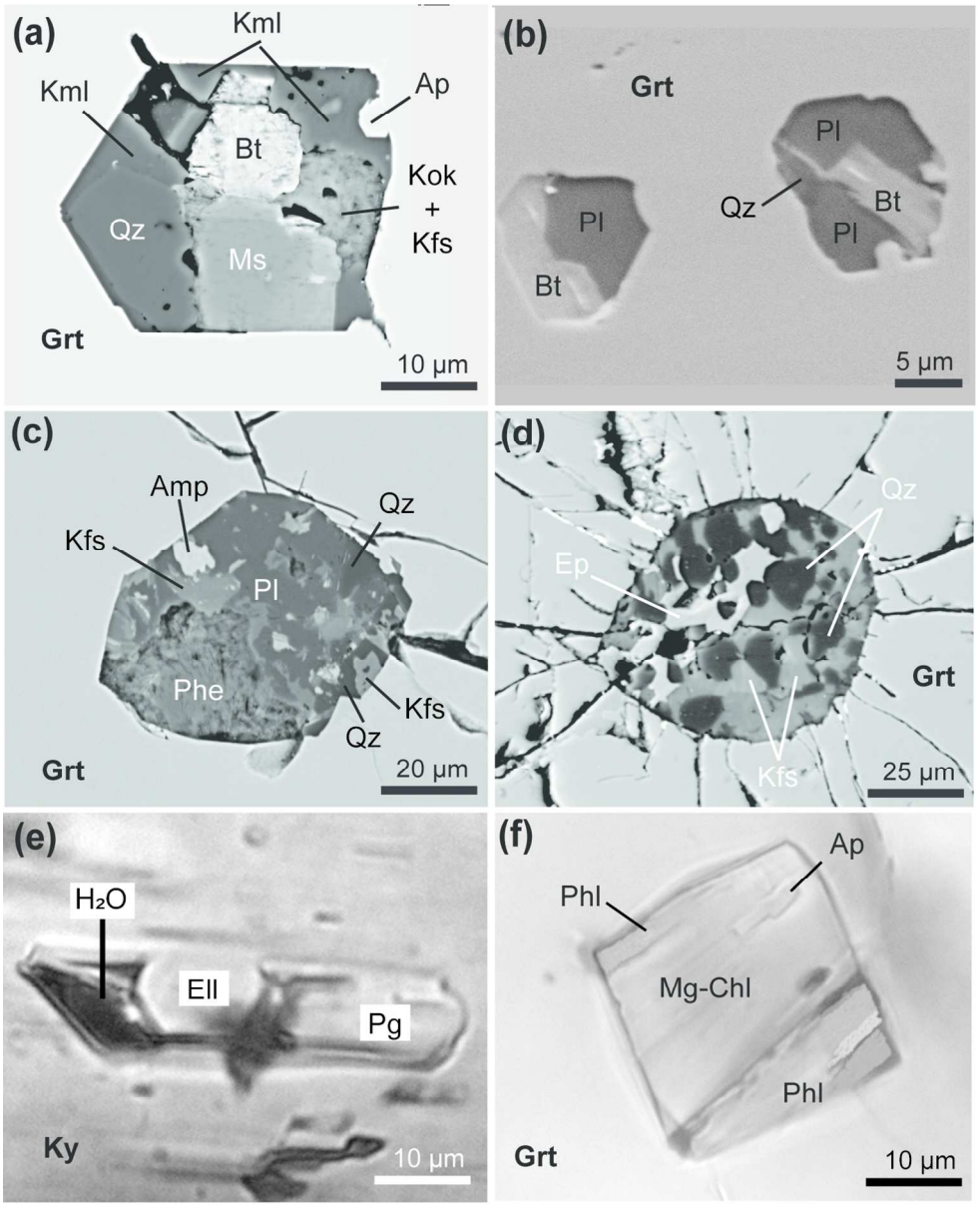

Figure 8: Polycrystalline inclusions interpreted as former melt droplets in HP/UHP rocks, BSE images. (a) Nanogranitoids from Polish Sudetes, Bohemian Massif (modified after Ferrero et al. 2016). Kml= kumdykolite; Kok= kokchetavite; (b) MSI from Kokchetav Massif, Kazakhstan (image courtesy of A.Stepanov, modified after Stepanov et al. 2016); (c) and (d) MSI from Shuanghe UHP eclogites, Dabie-Sulu orogeny. Image (c) was provided by Q.Liu and modified after Liu et al., 2013, while (d) is from Gao et al. 2013. (e) fluid inclusion in eclogite-facies Dora Maira whiteschists, modified after Ferrando et al. (2009); (f) multiphase solid inclusion in eclogite-facies Dora Maira whiteschists, modified after Frezzotti & Ferrando (2007).

120x148mm (300 x 300 DPI)

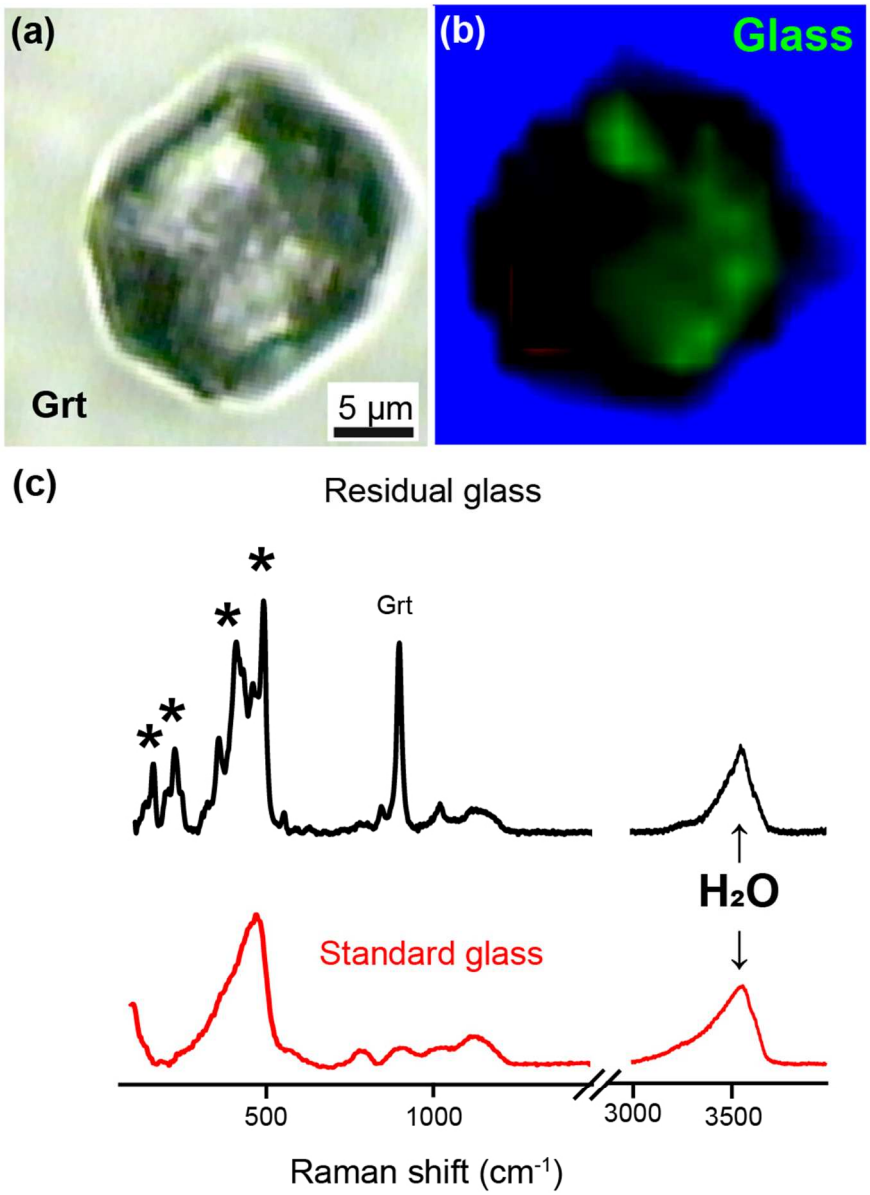

Figure 9: Residual glass in near-UHP nanogranitoids from the Polish Sudetes. (a) Nanogranitoid containing (b) residual glass, as visible from the Raman map of the spectral region 3200-3600 cm-1 characteristic of H2O hosted in glass (modified after Ferrero et al. 2016); (c) Raman spectrum of residual glass in near UHP nanogranitoids (modified after Ferrero et al. 2015). The main peaks of garnet are reported, along with peaks characteristic of other mineral phases crystallized in nanogranitoids (stars). A hydrous standard glass of granitic composition is reported for comparison (Morgan & London, 2005).

85x113mm (300 x 300 DPI)

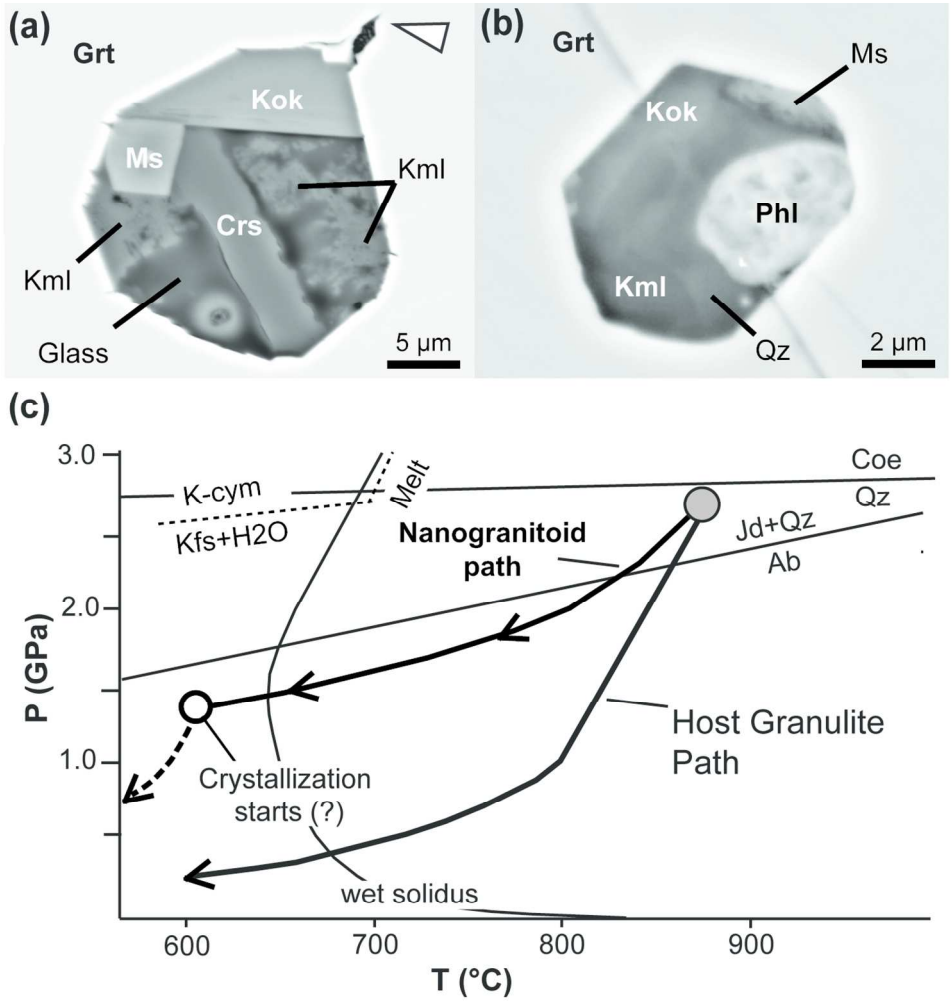

Figure 10: Metastable polymorphs crystallized in nanogranitoids from different HP rocks of the Bohemian Massif. (a) BSE images of inclusion in the Orlica-Śnieżnik granulites, modified after Ferrero et al. (2016); (b) inclusion in garnet clinopyroxenites of the Granulitgebirge (image courtesy of A. Borghini); (c) PT path followed by nanogranitoids in Orlica-Śnieżnik felsic granulites (modified after Ferrero et al., 2016) during cooling. Gray dot: minimum conditions for entrapment ~875°C and ~2.7 GPa (Ferrero et al., 2015), for reactions and solidus curves see Ferrero et al. (2016). The nanogranitoid path (thick line) is calculated assuming no crystallization even after the path crosses the wet solidus, when the melt enters in an undercooled state. When crystallization ultimately starts (white circle) well below the wet solidus, the Pinc drops significantly (dashed line). The T at which crystallization starts is only assumed, as it cannot be easily calculated given our present state of knowledge.

127x127mm (300 x 300 DPI)

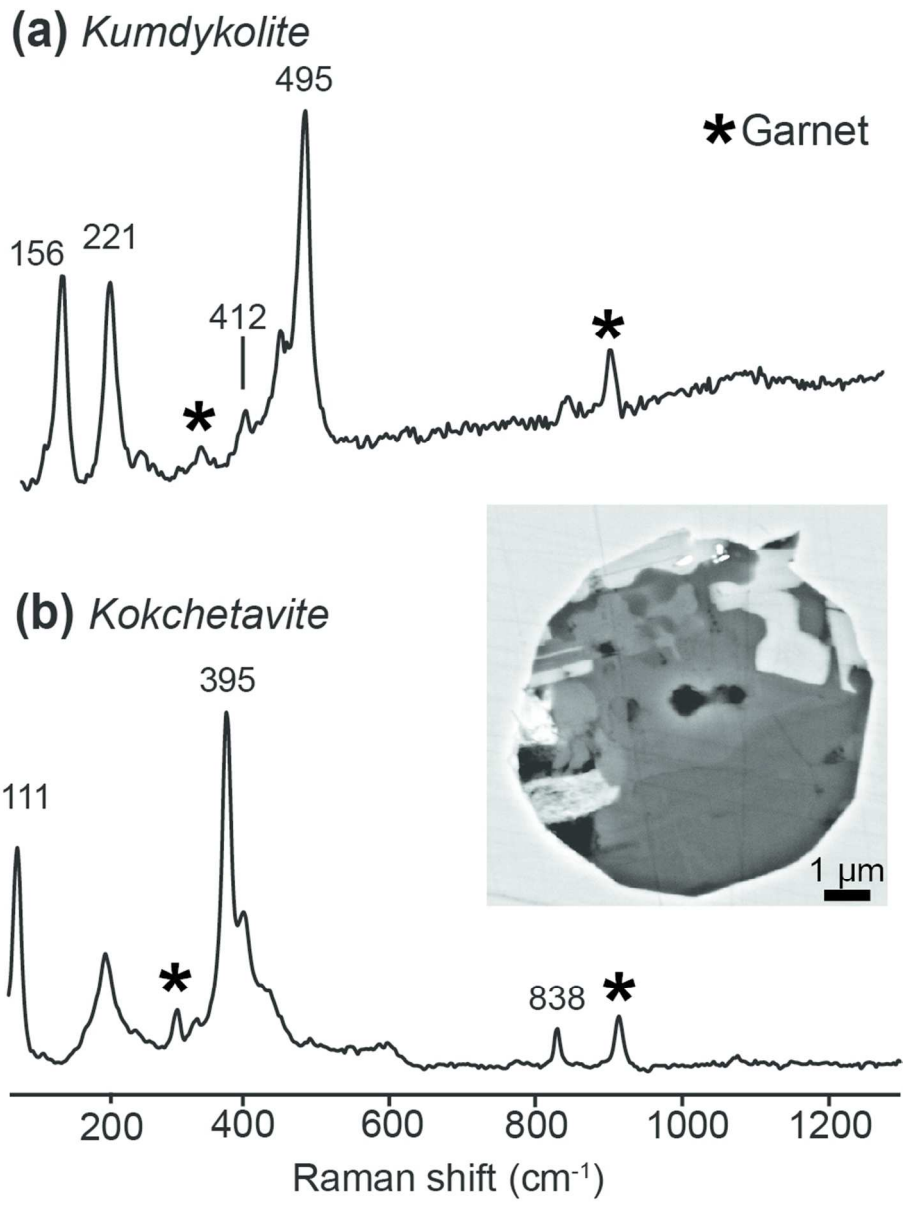

Figure 11: Characteristic Raman spectra of (a) kumdykolite and (b) kokchetavite in low P nanogranitoids from La Galite Archipelago (Ferrero, unpublished; BSE image modified after Ferrero et al., 2014).

83x110mm (300 x 300 DPI)

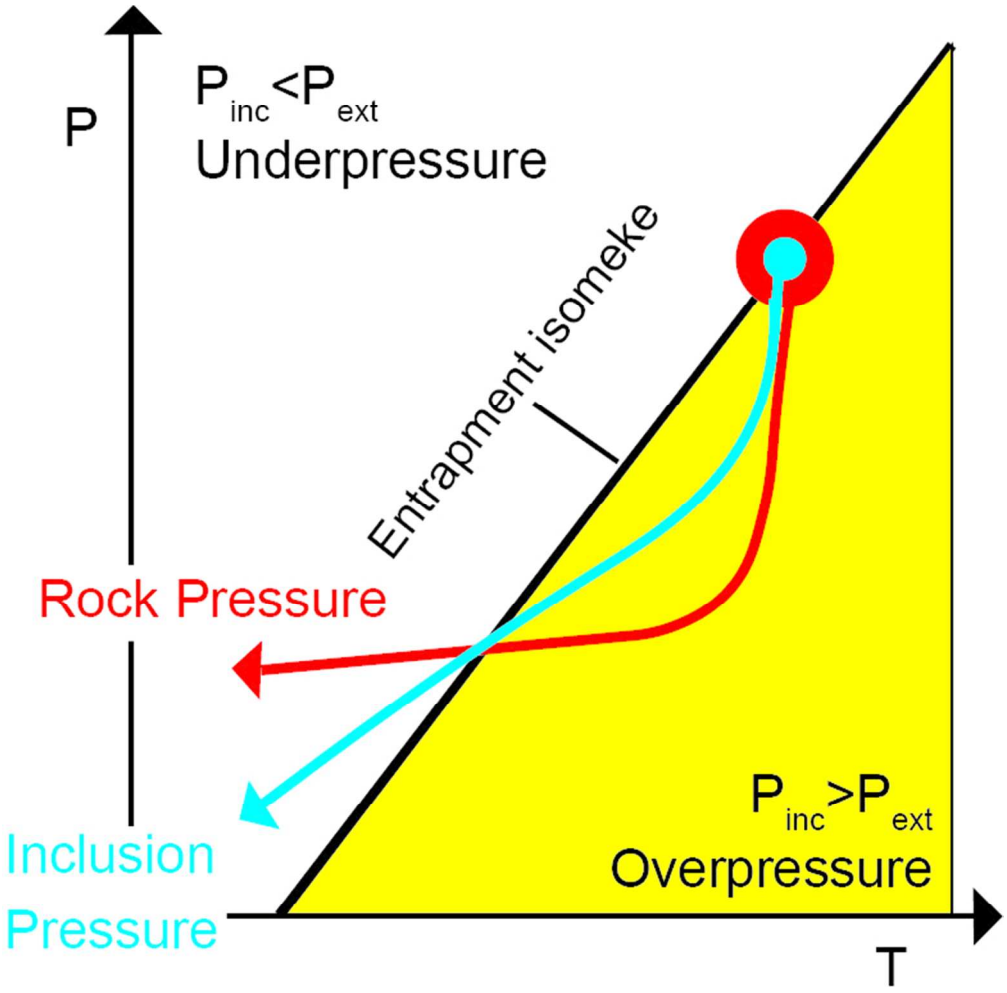

Figure 12. Qualitative diagram illustrating the evolution of the internal pressure for melt inclusions in garnet with respect to the entrapment isomeke. The pressure in an inclusion (blue line) that is softer than its host, as for MI in garnet, always remains between the external pressure (red line) and the pressure of the entrapment isomeke at the same T. When the rock pressure is below the entrapment isomeke, the inclusion is over-pressured. When the external pressure crosses the entranpment isomeke, the pressure in the inclusion is equal to the external pressure. When the external pressure lies above the entrapment isomeke, the inclusion is at a lower pressure.

66x65mm (300 x 300 DPI)

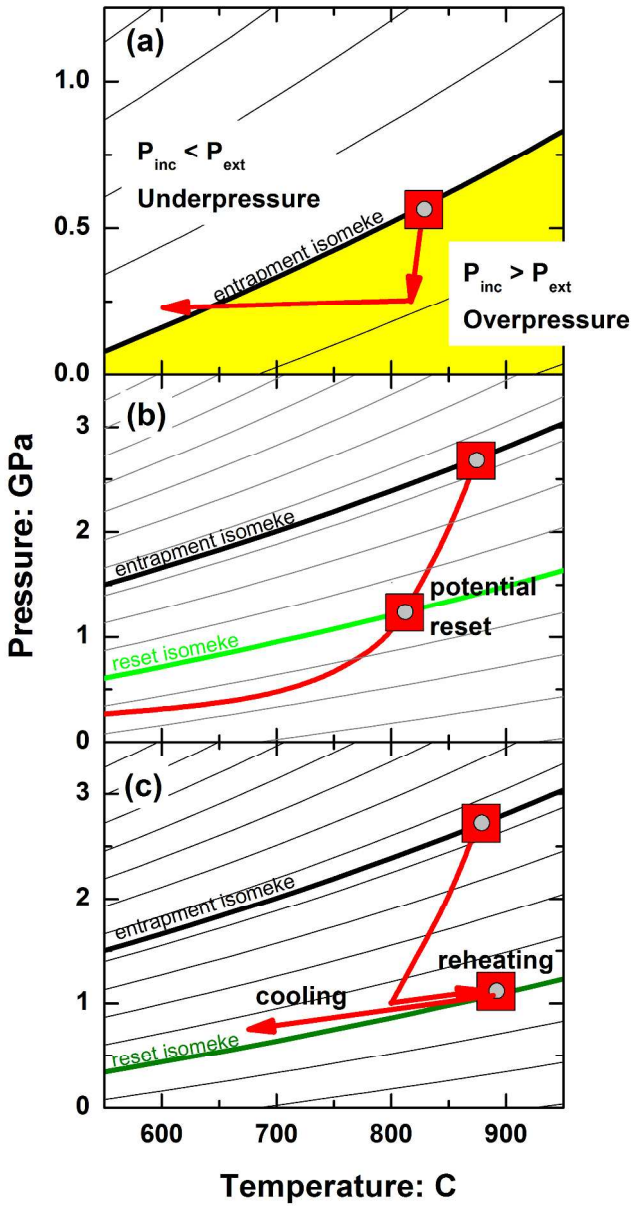

Figure 13. Principles of MI pressures illustrated with isomekes (thin lines) for MI in garnets with compositions from Ferrero et al. (2016). Key isomekes highlighted with green lines, rock P-T path with solid red lines (a) Entrapment at low P allows the rock path to take the inclusion to a condition of under-pressure by isobaric cooling after exhumation to shallow crustal levels, and thus promote the crystallisation of low-density 'metastable' polymorphs as the thermodynamically-stable phase in the inclusion. (b) Entrapment at HP conditions (example path taken from Fig. 10c) does not allow the rock path cross the entrapment isomeke, nor to cross an isomeke representing elastic resetting at lower pressures. (c) Reheating of the rock, for example during underplating, followed by quasi-isobaric cooling, can lead to under-pressure in the inclusion and the crystallisation of low-density phases.

199x371mm (300 x 300 DPI)

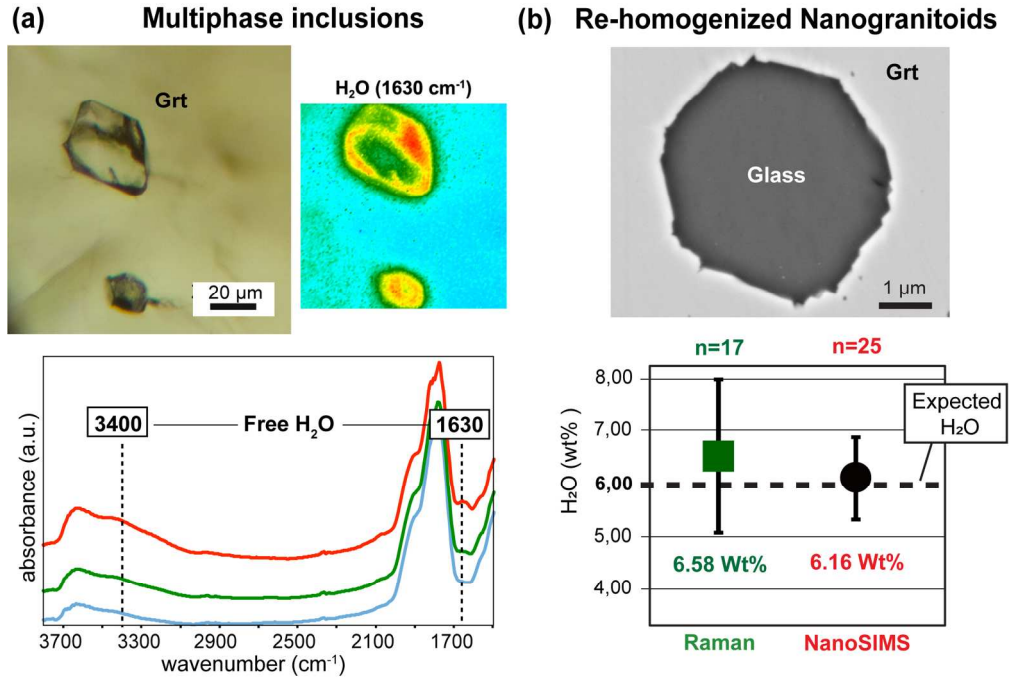

Figure 14. Preserved water in inclusions from HP/UHP rocks. (a) FTIR-FPA map of MSI in garnet orthopyroxenites from Dabie Shan (image modified after Malaspina et al. 2017). The map shows the intensity of the H2O band at 1630cm-1, indicated in the spectrum.For more details on the map, see Malaspina et al. (2017); (b) BSE image of re-homogenized nanogranitoids in garnet (modified after Ferrero et al. 2015) and a plot of measured H2O contents by Raman and NanoSIMS. The irregular shape of the nanogranitoid is not the result of any interaction with the host, since the chemical composition of the inclusion does not show any evidence of contamination from the host garnet.

163x110mm (300 x 300 DPI)

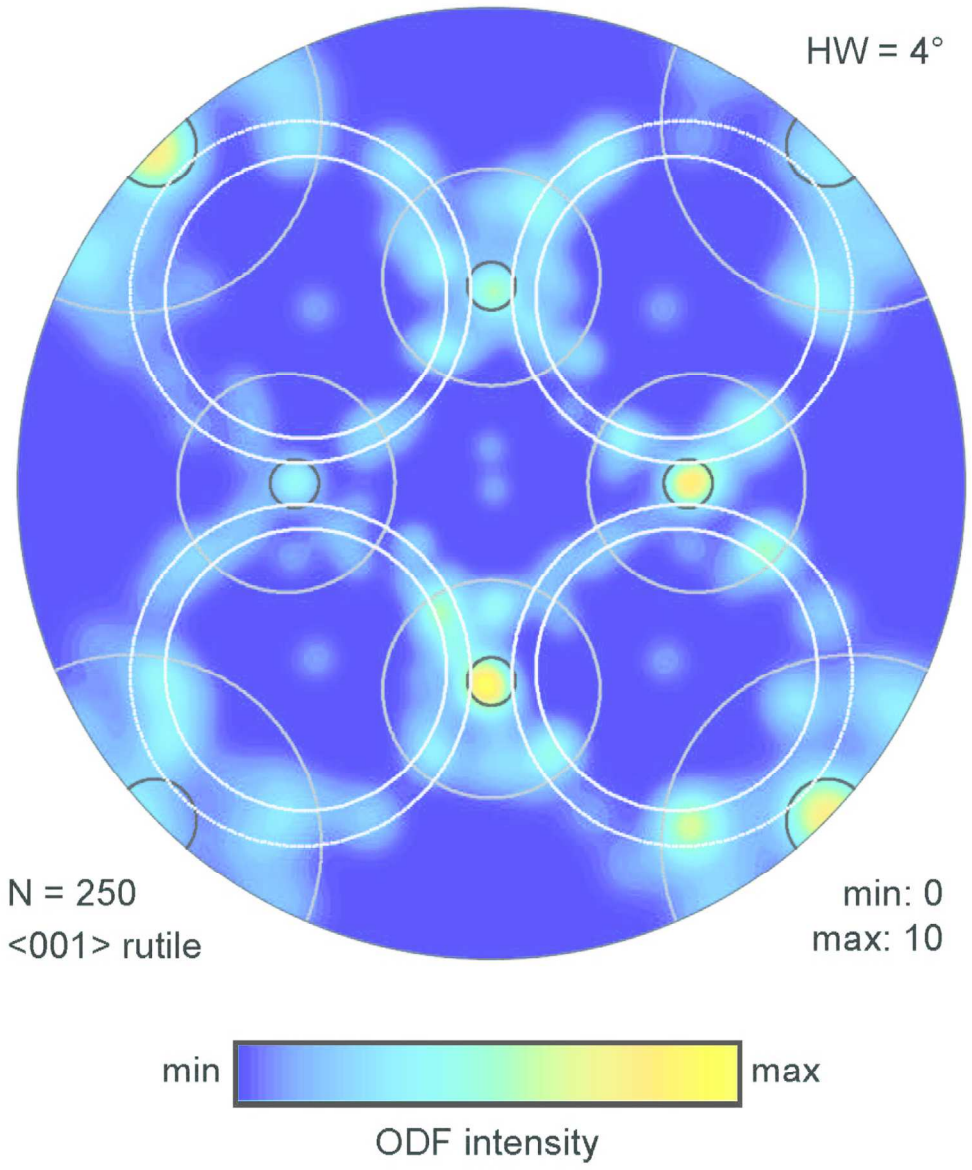

Figure 15: Equal angle stereographic projection of the orientation distribution function (ODF) of the c-directions of 250 rutile inclusions in two grains of a pegmatitic garnet, relative to the garnet unit-cell axes (Griffiths et al. 2016). The symmetry of the ODF reflects the symmetry of the garnet host crystal. The rutile inclusions clearly exhibit three distinct types of COR with respect to the garnet. One group of c-directions occurs in a small circle surrounding a high-symmetry direction in garnet (white circles). The second group (black circles) is a dispersional COR concentrated narrowly around a different high symmetry garnet direction. Surrounding this group a more diffuse concentration of c-directions is found (grey circles). For full details of the analysis see Griffiths et al. (2016).

134x159mm (300 x 300 DPI)